Co-Te mineralization in iron skarns on Vancouver Island and Texada Island

Wyatt M. Bain[1, a], Freia de Waal[1], and Dylan J. Goudie[2]

[1] British Columbia Geological Survey, Ministry of Mining and Critical Minerals, Victoria, BC, V8W 9N3
[2] Core Research Equipment and Instrument Training (CREAIT) Network, Memorial University of Newfoundland, 45 Arctic Avenue, St. John's, NL, A1C 5S7
[a] corresponding author: Wyatt.Bain@gov.bc.ca

Recommended citation: Bain, W.M., de Waal, F., and Goudie, D.J., 2025. Co-Te mineralization in iron skarns on Vancouver Island and Texada Island. In: Geological Fieldwork 2024, British Columbia Ministry of Mining and Critical Minerals, British Columbia Geological Survey Paper 2025-01, pp. 153-175.

Abstract

Iron skarns commonly contain Co along with base and precious metals. Vancouver Island, Texada Island, and Haida Gwaii in southern Wrangel have the largest concentrations of Co-bearing iron skarns in British Columbia. Here we present scanning electron microscopy-mineral liberation analysis (SEM-MLA) data showing the distribution and mineralogy of Co and Te in magnetite skarn, massive magnetite-calcite, podiform sulphide, and massive sulphide mineralization and associated alteration from iron skarns on Vancouver Island and Texada Island. Cobalt occurs primarily as cobaltite and is most commonly observed with sulphide-bearing quartz-carbonate-hornblende that crystallized after massive magnetite. In most cases, massive magnetite and sulphide-bearing orebodies are surrounded by proximal andradite-rich skarn and distal sodic-calcic alteration surrounding feldspar-scapolite veins. Bismuth-Ag-Hg telluride, electrum, and native bismuth are also commonly intergrown with cobaltite mineralization and occur as inclusions in primary pyrite-pyrrhotite-chalcopyrite.

Keywords: Skarn, iron skarn, cobalt, tellurium, bismuth, critical minerals, Wrangel terrane

1. Introduction

Cobalt is an essential component of rechargeable batteries and superalloys and cannot be substituted in most industrial applications (Dehaine et al., 2021). Similarly, tellurium is a key material for photovoltaic cells and thermoelectric devices (Goldfarb, 2015) and cannot be substituted without significant loss of efficiency and product performance (USGS, 2024). Therefore, disruptions in the availability of Co and Te represent risks to manufacturing supply chains and the global economy. Canada and most of its trading partners identify these elements as critical minerals (Nassar et al., 2022; Hickin et al., 2024; NRCan, 2024), and there is an ongoing effort to locate and develop domestic Co and Te resources.

Iron skarns (e.g., Cox, 1986) commonly contain primary Fe, Cu, and Au-Ag mineralization (Slack et al., 2017) with minor amounts of Co that can be refined as a co-product or by-product of base-metal refining (Mudd et al., 2013) such as at Cornwall, Pennsylvania (Lapham, 1968). The southern part of Wrangel terrane on Vancouver Island and Texada Island (Fig. 1; Hancock, 1988; Ray, 2013), an area that includes territories of many Indigenous Nations, hosts the largest concentration of iron skarns in British Columbia. Many of these occurrences were mined and prospected for base and precious-metal resources (Ray, 2013) but might also contain previously unrecognized Co mineralization.

Minerals containing Co and Te commonly constitute only a trace volume of base- and precious-metal mineralization

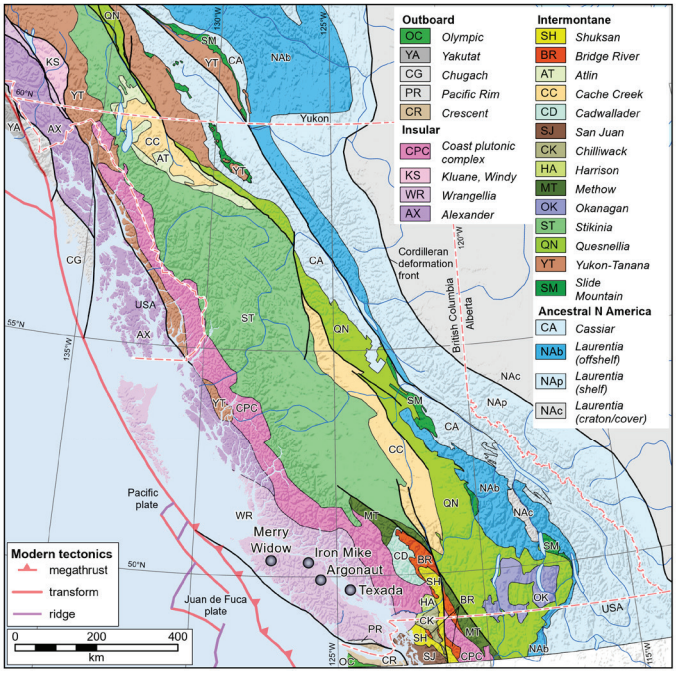

Fig. 1. Location of iron skarn clusters on Vancouver Island and Texada Island. Terranes modified from Colpron (2020).

(Hickin et al., 2024), and robust mineralogical data are commonly lacking at the deposit scale. This is partly due to the relative rarity of minerals in which these elements are major

constituents and identifying these minerals using conventional petrography. Automated scanning electron microscope-mineral liberation analysis (SEM-MLA) can be used to systematically identify micro-scale mineralogy and textural features in thin sections (e.g., Wang et al., 2022a, b; Liang et al., 2023; Shan et al., 2023). In this paper, we present SEM-MLA data documenting the occurrence of minerals containing Co and Te and describe their association with ore and alteration types in iron skarns from southwestern British Columbia (Fig. 1; Table 1).

2. Iron skarns

Skarns are generally classified as garnet- and pyroxene-rich calc-silicate rocks that replace or overprint host rocks adjacent to intrusions, within shear zones, or along faults. Skarns always have a genetic association with a source of heat (e.g., magmatic, tectonic) or fluids (e.g., hydrothermal, metamorphic) and can form in any rock type, but are most commonly associated with carbonate-rich sedimentary sequences (Meinert et al., 2005).

Skarns form via a continuum of metamorphic and metasomatic processes. Initially, skarn formation involves thermal isochemical metamorphism with no external mass transfer or exchange (Meinert et al., 2005). This results in the conversion of impure carbonate rocks to fine-grained, biotite-bearing calc-silicate hornfels and micro-scale exchange reactions between carbonate and interbedded silt and shale to produce reaction skarn (Zarayskiy et al., 1987). At this stage, the chemical character of the host rock is the primary control on the composition of skarn minerals, with magnesium- and calcium-rich host rocks producing magnesian and calcic skarn varieties.

The onset of mass transfer via magmatic or metamorphic fluid flux marks the transition from isochemical metamorphism to metasomatism (Meinert et al., 2005). Though host rock composition is still a primary control on skarn mineralogy at this stage, fluid composition and path of egress are the predominant constraints of the distribution and composition of skarn formed via metasomatic processes (Meinert et al., 2005). This initially produces skarnoid rocks via the coarsening of early-formed calc-silicates (Zharikov, 1970a, b). Subsequent fluid flux and mass transfer results in the wholesale conversion of host rocks into prograde anhydrous skarn assemblages of garnet and pyroxene and the transfer of metals and other elements to the skarn aureole from an external source (Newberry, 1991). Late-stage thermal collapse of the hydrothermal system and the influx of groundwater result in the retrograde formation of hydrous mineral assemblages rich in amphibole, epidote, chlorite, clays, carbonate, and quartz that overprint the anhydrous prograde assemblages (Newberry, 1991; Meinert et al., 2005). This retrograde stage is also commonly associated with the precipitation of sulphides introduced in the prograde phase (Ray, 2013). This pattern is consistent with a hydrothermal genetic model and applies well to most skarn varieties (e.g., Cu, Zn-Pb, W-Sn, Au-Ag; Einaudi et al., 1981; Dawson and Kirkham, 1996).

Like all skarns, iron skarn deposits have abundant calc-silicate alteration and commonly have a spatial relationship with a sources of heat such as an intrusion. However, iron skarns are distinguished by their magnetite-rich and silicate-poor character, their common spatial relationship with mafic intrusions and volcanic rocks, (Meinert et al., 2005; Ray and Webster, 2007), and their association with Co mineralization (Cox, 1986; Slack et al., 2017). Iron skarns are among the largest skarn deposit type and are typically mined for Fe, but can also contain significant Cu, Ni, and Au-Ag (Kesler, 1968; Vidal et al., 1990; Meinert et al., 2005).

3. Background

3.1. Geologic setting

Paleozoic-Mesozoic rocks of Wrangel terrane on Vancouver Island and Texada Island (Fig. 1) consist of arc-related intrusions, marine sedimentary rocks, and volcanic rocks (Fig. 2; e.g., Greene et al., 2006; Nixon and Orr, 2007; Canil and Morris, 2024). These rocks were accreted onto the western margin of North America during the late Jurassic or Early Cretaceous (e.g., Greene et al., 2006; Canil and Morris, 2024).

Basement rocks on Vancouver Island include the Paleozoic island arc volcanic and sedimentary rocks of the Nanoose complex and the Sicker and Buttle Lake groups (Sutherland Brown et al., 1986; Massey, 1995a-c). These rocks are overlain by Karmutsen Formation basalts, Quatsino Formation limestone, and other sedimentary units of the Vancouver Group (Middle to Late Triassic; Sutherland Brown et al., 1986; Nixon and Orr, 2007; Figs. 2, 3). The Bonanza Group overlies the Vancouver Group and includes the Parson Bay Formation (Upper Triassic to Middle Jurassic; DeBari et al., 1999; Nixon and Orr, 2007) which consists of siliciclastic and carbonate sedimentary rocks and arc-related volcanic rocks. The gabbroic to granodioritic intrusions of the Westcoast crystalline complex (ca. 190-174 Ma; DeBari et al., 1999; Canil et al., 2010) and diorite to granite intrusions of the Island Plutonic suite (ca. 201-166 Ma; Nixon et al., 2011a-d) were emplaced contemporaneously with, and in some areas overlain by, the Bonanza Group (Fig. 3; Canil et al., 2010). Bonanza Group rocks are overlain by, or are in fault contact with, the Coal Harbor Group, Longarm Formation (Lower Cretaceous), and Queen Charlotte and Nanaimo groups (Upper Cretaceous).

Similar geological relationships are preserved on Texada Island (Fig. 2b) where basement rocks include the Sicker and Buttle Lake groups (Paleozoic). These are overlain by lateral equivalents of the Karmutsen Formation and the Quatsino Formation. This stratigraphic sequence is intruded by diorite and quartz monzonite stocks associated with the Island Plutonic suite (Ettlinger and Ray, 1989; Webster and Ray, 1990a, b) and is overlain by the sedimentary rocks of the Nanaimo group (Cretaceous).

3.2. Deposit geology

Iron skarns on Vancouver Island and Texada Island,

Table 1. Orebodies in major iron skarn deposits on Vancouver Island and Texada Island.

Cluster, orebody	Lat./Long.	Description of the mineralization	Relationship with host rocks
Merry Widow cluster: Merry Widow-Kingfisher-Raven (Magnetite-calcite ±podiform sulphides)	50.3553, -127.2536	Massive magnetite-calcite with sulphide-bearing calcite-hornblende-quartz pods/ lenses.	Mineralization adjacent to the Coast Copper pluton (197.4-197.1 Ma), along the Kingfisher fault, and either replaces Bonanza Group volcanic rocks or forms pipe-like bodies that crosscut coarsely crystalline limestone.
Merry Widow cluster: Old sport (Magnetite skarn, podiform sulphides)	50.3789, -127.2378	Massive magnetite and garnet-epidote skarn overprinted with chalcopyrite-pyrrhotite-pyrite.	Mineralization pervasively replaces host rock along diorite sill that follows the brecciated contact between Karmutsen Formation volcanic rocks and Quatsino Formation limestones and likely extends down dip to the contact with the Coast Copper intrusion.
Merry Widow cluster: Marten, Copper Knob, Bluebird, Snowline, North Notch, Dry Hill, B3 (Massive sulphides)	50.3553, -127.2536	Massive pyrite-chalcopyrite-pyrrhotite surrounded by coarse calcite and open-space filling amphibole and quartz.	Mineralization along sharp contacts with coarse crystalline limestone immediately adjacent to mafic dikes of unknown age.
Argonaut cluster: Iron River (Magnetite skarn ±podiform sulphides)	49.9219, -125.4375	Massive magnetite with sulphide-bearing pods of quartz-hornblende-calcite-garnet. Sulphides are typically chalcopyrite-pyrite.	Mineralization ~0.5-1 km from a small granodiorite intrusion associated with the Quinsam intrusion (177 Ma; Island Plutonic suite) and primarily in epidote-chlorite altered volcanic rocks and interbedded sedimentary rocks of the Karmutsen Formation or Bonanza Group. Quatsino Formation limestones north of the main magnetite showing contains only minor magnetite mineralization.
Argonaut cluster: Argonaut/Iron Hill (Magnetite skarn ±podiform sulphides)	49.8622, -125.5458	Coarsely crystalline massive magnetite with garnet skarn gangue. Chalcopyrite mineralization is variable and contains minor Co.	Mineralization occurs within a hinge of an overturned syncline along a highly deformed contact between folded Karmutsen volcanic rocks and Quatsino Limestone near contact with the Quinsam granodiorite intrusion (177 Ma; IPS) that crosscuts both. Mineralization primarily replaces Karmutsen volcanic rocks near sharp contacts with crystalline limestone.
Argonaut cluster: Bacon Lake (Magnetite skarn, podiform sulphides)	49.9662, -125.6265	Podiform magnetite and pyrrhotite-pyrite-chalcopyrite in garnet-hornblende-clinopyroxene-epidote gangue. Sulphides host sporadic Co and Au-Ag.	Mineralization localized to pods of limestone and volcanic rock that are surrounded by apophyses of intrusive rock associated with nearby Island Plutonic Suite intrusions. Podiform orebodies occur along the irregular contacts between the volcanic and sedimentary rocks.
Iron Mike cluster: Iron Mike, TDH (Magnetite skarn ±podiform sulphides)	50.3083, -125.9789	Podiform bodies of massive magnetite separated by pods of garnet-epidote skarn. Little to no sulphides or other impurities other than calc-silicate gangue.	Mineralization focused along one or more bands (1-200 m thick) of crystalline, intravolcanic limestone within Karmutsen Formation pillowed basalt flows. Mineralization occurs ~0.5-1.5 km from the Adams River batholith (162.7 Ma, Island Plutonic suite).

Table 1. Continued.

Texada cluster: Volunteer, Spratt Bay (Magnetite skarn, podiform sulphides)	49.7443, -124.5123	Small bodies of massive magnetite minor chalcopyrite-pyrite-pyrrhotite and abundant garnet-pyroxene gangue. Locally enriched in Co and Au-Ag.	Mineralization occurs in 1-10 m thick bands of intervolcanic limestone within variably pillowed, amygdaloidal basalt flows (Karmutsen Formation). Mineralization is 1-3 km from a Cretaceous (?) granodiorite stock.
Texada cluster: Prescott, Lake, YKD, Paxton (Magnetite skarn, podiform and massive sulphides)	49.7047, -124.5489	Massive magnetite with abundant garnet-pyroxene-hornblende skarn and minor pyrite-chalcopyrite-pyrrhotite (podiform and massive sulphides).	In epidote-chlorite-altered Karmutsen Formation along a highly deformed contact between bleached white Quatsino Formation limestone and the Gillies Bay quartz monzonite stock (169 Ma; Island Plutonic suite) immediately to the east. Massive sulphides in coarse limestone and calcite pods immediately adjacent to mafic dikes.

are primarily calcic in composition and form clusters of occurrences with the same general geology, host rocks, and cross-cutting relationships (Ray, 2013; Table 1). The upper part of the Karmutsen Formation represents the oldest rocks in every deposit and consists of green-black, fine-grained, massive, amygdaloidal basalt flows and pillowed volcanic rocks. In many areas, the upper part of the Karmutsen Formation contains one or more 1-200 m thick beds of inter-volcanic limestone (Fig. 3). These volcanic rocks and the limestone beds are common hosts for iron skarn mineralization (Fig. 3; Table 1). Karmutsen Formation-hosted iron skarns include those in the Iron Mike, Texada, and Argonaut clusters (Table 1; Fig. 2).

The structural contact between the Karmutsen Formation and overlying Quatsino Formation rocks is a common location for iron skarn formation (e.g., Prescott, Paxton, YKD, Lake; Table 1). This contact is deformed and brecciated and pervasively altered to magnetite skarn and overprinted with secondary sulphides (Sangster, 1969; Ray and Webster, 1991). This deformation and overprinting is commonly so pervasive that the host-rock protolith is obscured (e.g., Old Sport, Table 1). In contrast, iron skarns in the massive limestones in the upper and middle parts of the Quatsino Formation are rare. These skarns typically form discrete pipe-like bodies with minor sulphides (e.g., Kingfisher in the Merry Widow cluster; Ray and Webster, 1991; Nixon et al., 2011d; Morris and Canil, 2020, 2024; Bain and Waugh, 2024). In all cases, calc-silicate alteration in the Quatsino is minor relative to Karmutsen or Bonanza Group rocks (e.g., Old Sport, Prescot, Paxton; Bain and Waugh, 2024).

The massive to thinly bedded volcaniclastic rocks and marine sedimentary rocks of the Parson Bay Formation at the base of the Bonanza Group (Nixon and Orr, 2007; Figs. 2, 3) also host significant iron skarn mineralization (e.g., Merry Widow, Raven, Iron River; Table 1). These rocks are commonly in unconformable contact with the underlying Quatsino Formation limestone and are overprinted by pale-green albite alteration (Bain and Waugh, 2024). As with the Karmutsen Formation, calc-silicate alteration is more pervasive in Bonanza Group rocks than the underlying limestone (Bain and Waugh, 2024).

Iron skarns on Vancouver Island and Texada Island are all spatially associated with Island Plutonic suite intrusions (e.g., the Coast Copper, Quinsam, Adams River, and Gillies Bay intrusions). These intrusions range from gabbro to granodiorite and have U-Pb zircon ages between 201 and 166 Ma (Nixon et al., 2011a-d). Phlogopite from the Merry Widow deposit has a K-Ar date of 197.9 ±1.3 Ma (Nixon et al., 2011d) that overlaps the zircon U-Pb date of ca. 197.4 ±0.5 Ma to ca. 197.1 ±0.3 Ma for the adjacent Coast Copper intrusion. These data, along with the common spatial association of Island Plutonic suite intrusions with iron skarns across the Wrangel Terrane, suggests a genetic relationship between the Island Plutonic intrusions and the associated skarns. However, Island Plutonic suite intrusions generally lack significant endoskarn mineralization and, where present, endoskarn commonly lacks clear continuity with exoskarn formed in adjacent volcanic and sedimentary rocks.

Multiple generations of fine-grained, sulphide-bearing mafic dikes and sills with well-defined chilled margins occur in and around the iron skarns (Bain and Waugh, 2024). These dikes commonly host Cu-Au-bearing massive sulphide mineralization, where they crosscut recrystallized limestone strata (Bain and Waugh, 2024). These massive sulphide bodies typically lack abundant skarn alteration like that observed in and around the massive magnetite orebodies. The associated dikes are likely coeval with or post-date Island Plutonic suite intrusions, but this relationship is typically unclear (Ray and Webster, 1991).

4. Methods

4.1. Sample selection

Forty-two samples from seven iron skarns were selected for this study (Table 2). These samples were taken from outcrops and drill cores that show characteristic ore and alteration minerals and their textures, associations, and cross-cutting

relationships. The sample suite includes volcanic host rocks overprinted with calc-silicate and sodic-calcic alteration and mineralized rocks (i.e., massive calc-silicate, massive sulphides, magnetite skarn, magnetite-calcite, and podiform sulphide mineralization styles).

4.2. Methods: scanning electron microscopy-mineral liberation analysis (SEM-MLA)

Quantitative mineral studies of 42 thin sections (30-100 µm) were conducted at CREAIT Microanalysis Facility at Memorial University using a FEI Quanta field emission gun 650 scanning electron microscope (SEM) equipped with mineral liberation analysis (MLA) software version 3.14 (Sylvester, 2012; Grant et al., 2018; Beranek et al., 2023). Instrument conditions included a 25 kV accelerating voltage, 13.5 mm working distance, and 10nA beam current. The MLA frames were 1.5 by 1.5 mm with a resolution of 500 by 500 pixels. Backscatter electron (BSE) images (Fig. 4b) of each frame were used to identify features to a resolution of 30 µm or less, depending on the contrast in BSE signal across mineral grain boundaries. MLA maps (Fig. 4c) were created using GXMAP mode by acquiring energy-dispersive X-ray spectra in a grid every 10 pixels, with a spectral dwell time of 12 ms, and comparing these against an in-house library of mineral reference spectra. The accuracy of mineral identification was verified using in situ imaging and point analysis. Each MLA dataset was first rendered with unique colours representing every mineral phase (Fig. 4c). A custom colour scheme that groups or subdivides mineral groups based on their composition and paragenesis (Figs. 4d, 5) was then chosen to highlight textural features and cross-cutting relationships.

Subsequent processing of MLA data in Adobe Photoshop isolated pixel groups (i.e., minerals) in each MLA scene to evaluate the paragenesis of the mineral phases they represent. Isolated pixels were grouped and rendered in colour (Fig. 4e) and black and white panels (Fig. 4f) to show the distribution of paragenetic assemblages within the analyzed samples. Mineral phases containing elements identified on the 2024 version of the Canadian critical mineral list (NRCan, 2024) were highlighted to show their distribution in the paragenetic assemblages (Fig. 4g).

5. Results

The mineralogy, textures, and distribution of critical minerals was evaluated on a pixel-by-pixel basis and yielded similar results across all the studied deposits.

5.1. Mineralization

On the metre scale, mineralization is variable and commonly includes three styles: 1) magnetite skarn, 2) massive magnetite-calcite, and 3) sulphide. These styles vary in abundance between deposits and were often transitional between one another. For instance, magnetite skarn and massive magnetite-calcite commonly grade into each other and both styles contain variable podiform sulphides.

5.1.2. Magnetite skarn mineralization

Magnetite skarn is the most common mineralization style across all deposits and occurs as zones of intergrown calc-silicate minerals and magnetite that replace host rocks. This style is primarily developed in fragmental volcanic rocks (i.e., the Karmutsen and Parson Bay formations) and composed of prograde clinopyroxene-garnet and magnetite overprinted with prograde carbonate-hornblende, all of which replace host rocks (Fig. 6a). The prograde clinopyroxene (i.e., diopside-hedenbergite; Ray, 2013) pervasively replaces the cores of host rock fragments that are surrounded by coarse magnetite and garnet along their outer edges (Figs. 6b, c). The garnets are typically euhedral with well-developed growth zones (Figs. 6c, 7a, c) defined by intergrown amphibole-carbonate (i.e., hornblende, actinolite, and calcite; Figs. 6c, d, f). Garnets are primarily andradite-grossular but are most commonly andradite-rich in sulphide-rich samples (Figs. 6c-e, 7). Chlorite-epidote commonly overprint the clinopyroxene, garnet, and magnetite that replace host rock fragments and are likely part of a retrograde assemblage (Fig. 6b)

Sulphide minerals are almost always intergrown with retrograde quartz-carbonate-hornblende ±clinopyroxene ±magnetite (Figs. 6d-g). The sulphides comprise aggregates of coarse pyrite-pyrrhotite-chalcopyrite with minor amounts of bornite-cuprite-cobaltite-pentlandite-arsenopyrite (Figs. 6f, g). Minor amounts of sulphides are also intergrown with fine-grained, prograde magnetite, but this is rare.

Minerals containing Co and Te are generally in low abundance in magnetite skarn mineralization. However, sporadic zones of course primary cobaltite intergrown with garnet and magnetite are in limestone beds in the upper part of the Karmutsen Formation on Texada Island (Fig. 7).

5.1.3. Massive magnetite-calcite mineralization

Massive magnetite-calcite (Table 1) comprise orebodies of pure magnetite and interstitial calcite with abundant open space-filling textures (Bain and Waugh, 2024). These orebodies are surrounded by skarn developed in volcanic rocks (e.g., Merry Widow orebody) and form pipe-like bodies with minor abundances of calc-silicate minerals and sharp contacts with host rock when formed in limestone (e.g., Kingfisher orebody; Bain and Waugh, 2024).

Primary magnetite in magnetite-calcite orebodies occurs as masses of fine-grained crystals surrounded by coarse euhedral crystals with open space-filling, botryoidal textures (Fig. 8). Open space-filling magnetite is enveloped by 1-5 cm thick masses of retrograde carbonate-hornblende-quartz±chlorite±epidote and variable orthopyroxene and orthoclase intergrown with the retrograde minerology. This retrograde assemblage fills interstitial space and fractures in magnetite and is the most common context for pyrite-pyrrhotite-chalcopyrite-arsenopyrite and other sulphides (Figs. 8c, b) in mineralized rocks across all deposits.

Cobalt sulpharsenides and telluride minerals occur in massive magnetite-calcite orebodies and are always associated with Fe-

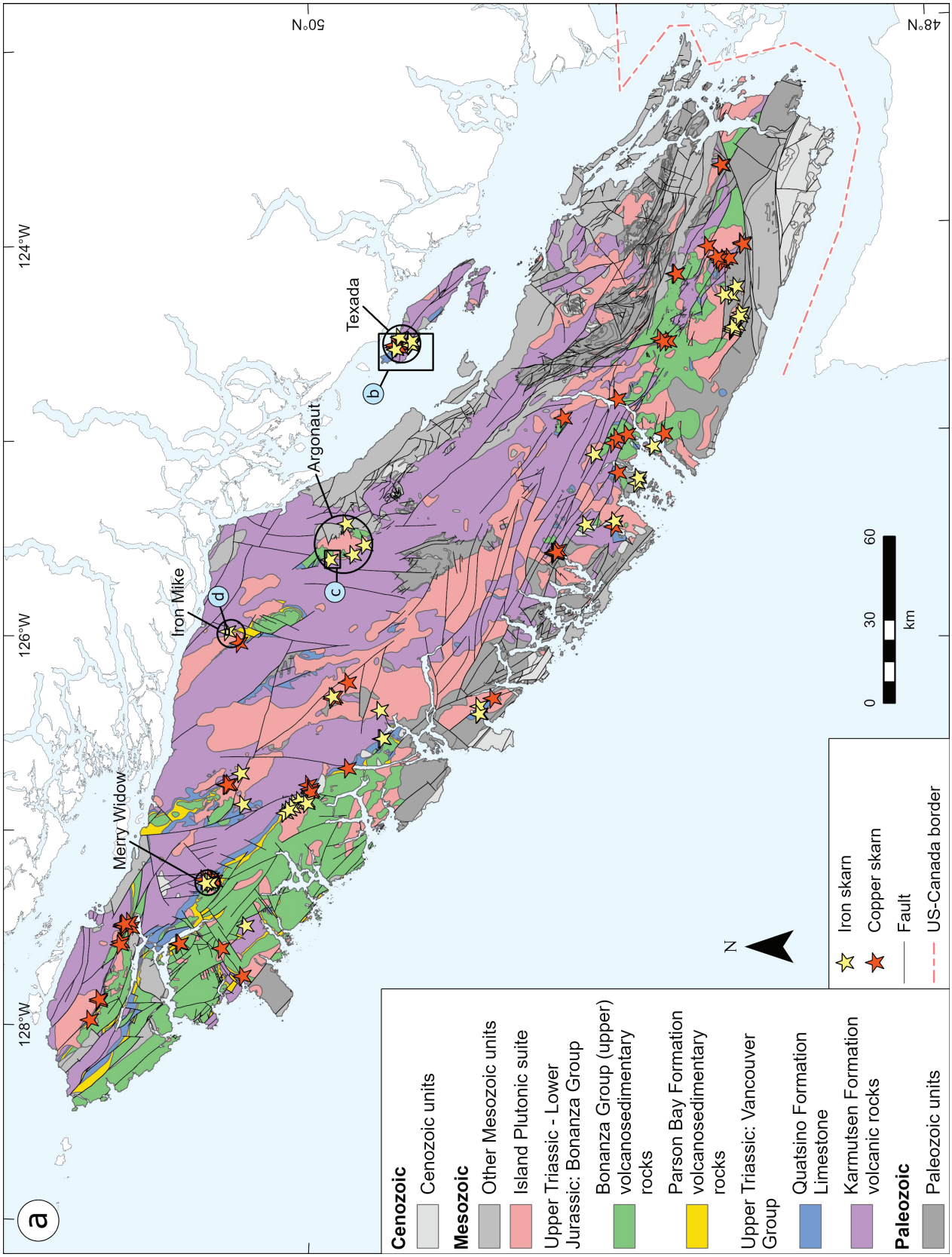

Fig. 2. a) Generalized geology of Vancouver Island showing locations of iron skarn deposits and the iron skarn clusters discussed in this paper. Modified after Cui et al., 2017. **b)** Geologic map of northern Texada Island showing the Texada iron skarn cluster. Skarn outlines are too small to be represented at the scale of this map. **c)** Geologic map of the northwestern portion of the Argonaut iron skarn cluster showing the Bacon Lake deposit. Modified from Ferguson, 2021. **d)** Geologic map of the southern portion of the Iron Mike iron skarn cluster. Modified from Shearer, 2007.

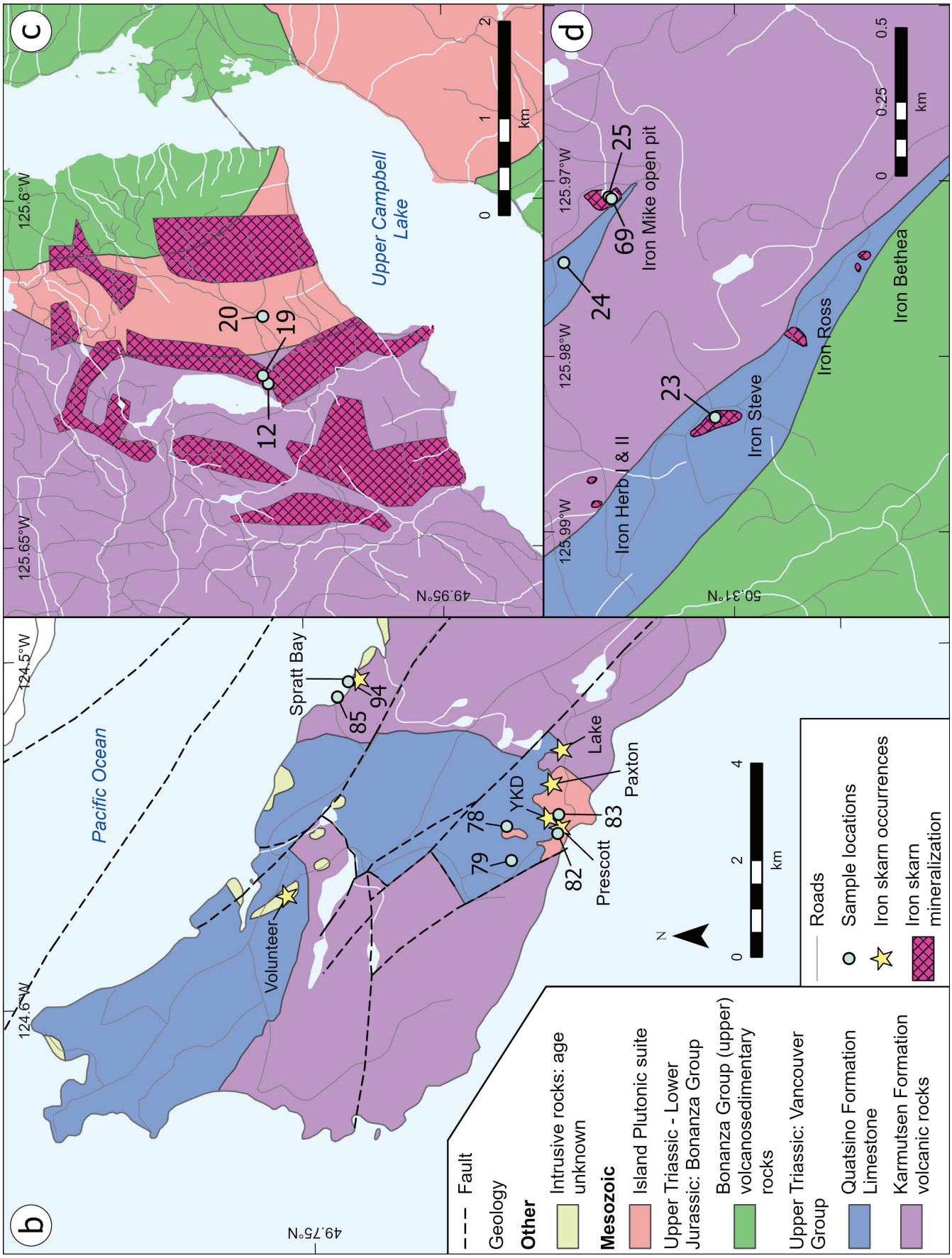

Fig. 2. Continued.

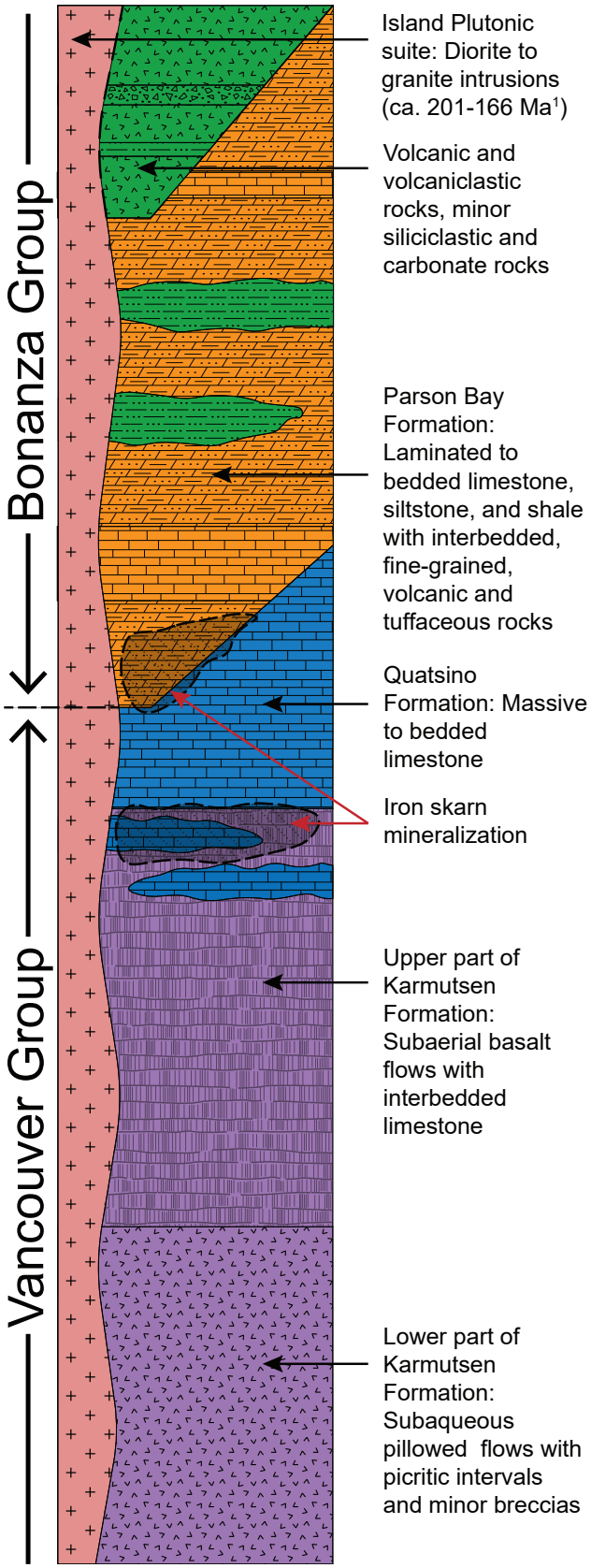

Fig. 3. Schematic stratigraphy of Vancouver Island showing the stratigraphic context of iron skarns. Modified from Nixon and Orr (2007) and Canil et al. (2010). [1] Ages from Nixon et al. (2011a-d).

and Cu-sulphides and retrograde calcite-hornblende-quartz (Figs. 8c, d) that crosscut massive magnetite (Figs. 9a-c). Cobaltite is the most common sulpharsenide and is commonly intergrown with pyrite, pyrrhotite and calcite (Figs. 8, 9). Silver-bismuth tellurides are commonly intergrown with cobaltite (Fig. 9d) or form inclusions in pyrrhotite and pyrite along with native bismuth and electrum.

5.1.4. Sulphide mineralization

Sulphide mineralization varies from podiform to massive (Bain and Waugh, 2024). These morphological styles have similar bulk sulphide mineralogy but form in distinct settings and have different trace metal contents.

Podiform sulphide ores comprise aggregates of euhedral to anhedral pyrite-chalcopyrite-pyrrhotite (Fig. 10) with minor magnetite, arsenopyrite, pentlandite, sphalerite, galena, and rare bornite-chalcocite-cuprite. This morphological variant occurs within massive magnetite skarn and magnetite-calcite orebodies and is always intergrown with or crosscut by coarse retrograde carbonate-hornblende-quartz-chlorite-epidote±magnetite and minor amounts of intergrown orthopyroxene (Figs. 10a-c). Podiform sulphides resemble the sulphide-bearing carbonate-hornblende-quartz masses associated with open space-filling magnetite in the magnetite-calcite orebodies but are more sulphide-rich (>25 vol.% sulphides) and larger (>1 m wide).

Massive sulphide ores are >60 vol.% sulphides, which form veins and discrete masses with minor silicate-oxide gangue along the margins of mafic dikes (Ray and Webster, 1991; Travis et al., 2022; Bird, 2023; Bain and Waugh, 2024). This mineralization style lacks replacement textures and occurs exclusively along the contact between crystalline limestone and mafic dikes. The dikes associated with this style are gabbro to monzogabbro, 0.5-4 m wide in cross section, and overprinted with epidote-chlorite±orthoclase alteration (Bain and Waugh, 2024). The sulphide assemblage generally consists of pyrite-chalcopyrite-pyrrhotite-arsenopyrite-bornite-chalcocite and minor cuprite, pentlandite, and sphalerite (e.g., Marten and Copper Knob; Table 1), but some are predominantly pyrite-chalcopyrite (Figs. 11a, b) and others 30-50% arsenopyrite (e.g., B3; Figs. 11c, d). Due to their lack of replacement textures, massive texture, general lack of abundant calc-silicate minerals, and occurrence outside of massive magnetite or skarn bodies, the paragenesis of the massive sulphide ores is unclear.

Primary pyrite and pyrrhotite in podiform sulphides contain Ag-Bi tellurides and electrum inclusions. Cobaltite, cobalt-arsenic hydroxide (erythrite), and native Bi are also common and occur with secondary fracture-filling carbonate-hornblende-quartz and chlorite-orthopyroxene-limonite veinlets that crosscut primary sulphides (Figs. 10c-e).

Primary pyrite-pyrrhotite-chalcopyrite-arsenopyrite in massive sulphide bodies contain inclusions of Ag-Bi-Hg tellurides and minor electrum. Electrum and Ag-Bi tellurides are also common with secondary weathering products of massive sulphides (e.g., scorodite, Fig. 11). In this setting, Ag-Bi tellurides are restricted to secondary chalcopyrite-bornite-

Table 2. Samples analyzed and minerals identified by MLA in this study.

Sample Type	Sample ID	Deposit	Figure Label	Lat.	Long.	Cu	Au-Ag	Co	Te	Bi
Alteration Skarn	24WBA-158-019D	Bacon Lake	c; 19	49.97	-125.63			Co		
Alteration Skarn	S23WBA-008-a-7	Iron River	c	49.92	-125.44					
Alteration Skarn	S23WBA-021-a-4	Iron River	c	49.92	-125.44	Cu		Co		
Alteration Skarn	S23WBA-085-g	Spratt Bay	b; 85	49.74	-124.51			Co		
Alteration Skarn	S23WBA-094-b	Spratt Bay	b; 94	49.74	-124.51					
Alteration Na-Ca	S23WBA-059-d-2	Merry Widow	a	50.36	-127.25		Au-Ag			
Alteration Na-Ca	D23WBA-048-004	MW21-009	a	50.36	-127.25					
Alteration Na-Ca	D23WBA-048-017a	MW21-009	a	50.36	-127.25			Co		
Alteration Na-Ca	D23WBA-048-030	MW21-009	a	50.36	-127.25			Co		
Alteration Na-Ca	D23WBA-047-049	MW21-014	a	50.36	-127.25					
Magnetite skarn	24WBA-156-008A-4	Argonaut	c	49.86	-125.54	Cu		Co		
Magnetite skarn	24WBA-158-019G	Bacon Lake	c; 19	49.97	-125.63		Ag	Co	Te	Bi
Magnetite skarn	24WBA-158-019L	Bacon Lake	c; 19	49.97	-125.63				Te	Bi
Magnetite skarn	24WBA-160-024B-3	Iron Mike	d; 24	50.31	-125.98			Co		
Magnetite skarn	S23WBA-021-a-6	Iron River	c	49.92	-125.44					
Magnetite skarn	S23WBA-032-a-1	Old Sport	a	50.37	-127.24		Au-Ag			
Magnetite skarn	S23WBA-078-f	Paxton	b; 78	49.70	-124.54	Cu				
Magnetite skarn	S23WBA-083-d	Prescott	b; 83	49.70	-124.55	Cu	Au-Ag		Te	
Magnetite skarn	S23WBA-085-c	Spratt Bay	b; 85	49.74	-124.51			Co		
Magnetite skarn	S23WBA-082-d	YKD	b; 82	49.70	-124.55	Cu				
Host Bonanza Gp	S23WBA-059-g	Merry Widow	a	50.36	-127.25					
Host Karmutsen Fm	24WBA-160-023A-2	Iron Steve	d; 23	50.31	-125.99			Co		
Host Mafic Dike	D23WBA-048-017b	MW21-009	a	50.36	-127.25					
Magnetite-calcite	24WBA-156-006A-3	Argonaut	c	49.86	-125.54	Cu	Ag			
Magnetite-calcite	24WBA-157-012A-4	Bacon Lake	c; 12	49.97	-125.63		Au-Ag	Co	Te	Bi
Magnetite-calcite	24WBA-157-013A-3	Bacon Lake	c; 12	49.97	-125.63		Au-Ag	Co	Te	Bi
Magnetite-calcite	24WBA-158-020E	Bacon Lake	c; 20	49.97	-125.62			Co		
Magnetite-calcite	D23WBA-047-020	MW21-014	a	50.36	-127.25	Cu	Au-Ag	Co		
Magnetite-calcite	D23WBA-047-025	MW21-014	a	50.36	-127.25	Cu	Ag	Co	Te	Bi
Massive sulfide	S23WBA-031-a-1	B3	a	50.35	-127.25	Cu	Au-Ag		Te	Bi
Massive sulfide	S23WBA-079-c	Lafarge	b; 79	49.71	-124.56	Cu	Ag		Te	Bi
Massive sulfide	24WBA-162-027B-3	Marten	a	50.35	-127.25				Te	Bi
Podiform sulphides	24WBA-156-011A-2	Argonaut	c	49.86	-125.54					Bi
Podiform sulphides	24WBA-158-020C	Bacon Lake	c; 20	49.97	-125.62	Cu	Ag	Co	Te	Bi
Podiform sulphides	24WBA-158-020D	Bacon Lake	c; 20	49.97	-125.62	Cu		Co		
Podiform sulphides	24WBA-160-025A-3	Iron Mike	d; 25	50.31	-125.98					
Podiform sulphides	S23WBA-069-a-2	Iron Mike	d; 69	50.31	-125.98			Co		Bi
Podiform sulphides	D23WBA-047-029	MW21-014	a	50.36	-127.25	Cu	Au-Ag			Bi
Podiform sulphides	D23WBA-047-032	MW21-014	a	50.36	-127.25	Cu	Au-Ag		Te	Bi
Podiform sulphides	D23WBA-047-038	MW21-014	a	50.36	-127.25	Cu	Au-Ag	Co	Te	Bi
Podiform sulphides	S23WBA-032-b-1	Old Sport	a	50.37	-127.24	Cu		Co		

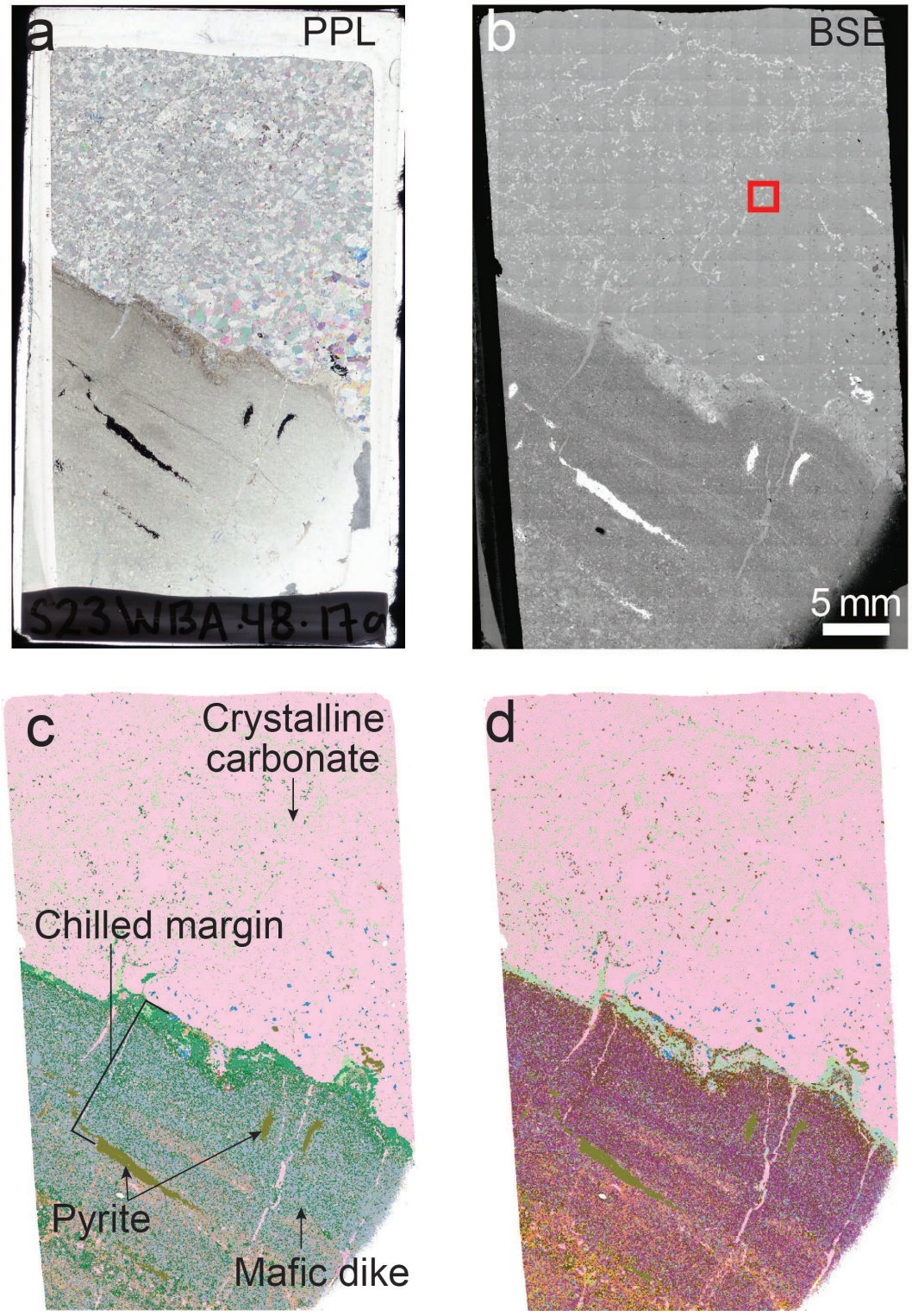

Fig. 4. Example of the workflow used to collect and process MLA data. This sample (S23WBA-48-17a) shows the contact between carbonate host rock and the sulphide-bearing chilled margin of a mafic dike from the Merry Widow deposit. **a)** Thin section in plain polarized light (PPL). **b)** BSE mosaic of the same thin section. A red square denotes the footprint of individual mosaic tiles. **c)** MLA map with each mineral represented as a unique colour. This image is generated using grain boundaries recognized in the BSE mosaic and a grid of energy-dispersive spectroscopy point data. **d)** MLA data rendered with a custom colour scheme (Fig. 5). **e)** Panels showing isolated pixel groups representing the mineral assemblages of the host carbonate, chilled margin, and transitional zone between the chilled margin and core of the mafic dike (Left: carbonate-clinopyroxene; Centre: albite-hornblende-chlorite-epidote; Right: intermediate plagioclase-orthoclase-sulphides). **f)** The same panels showing each mineral assemblage in uniform, monochromatic black. **g)** Inset image of the sulphide-rich area from the transitional zone illustrating the distribution of cobaltite (circled in red). See text for details.

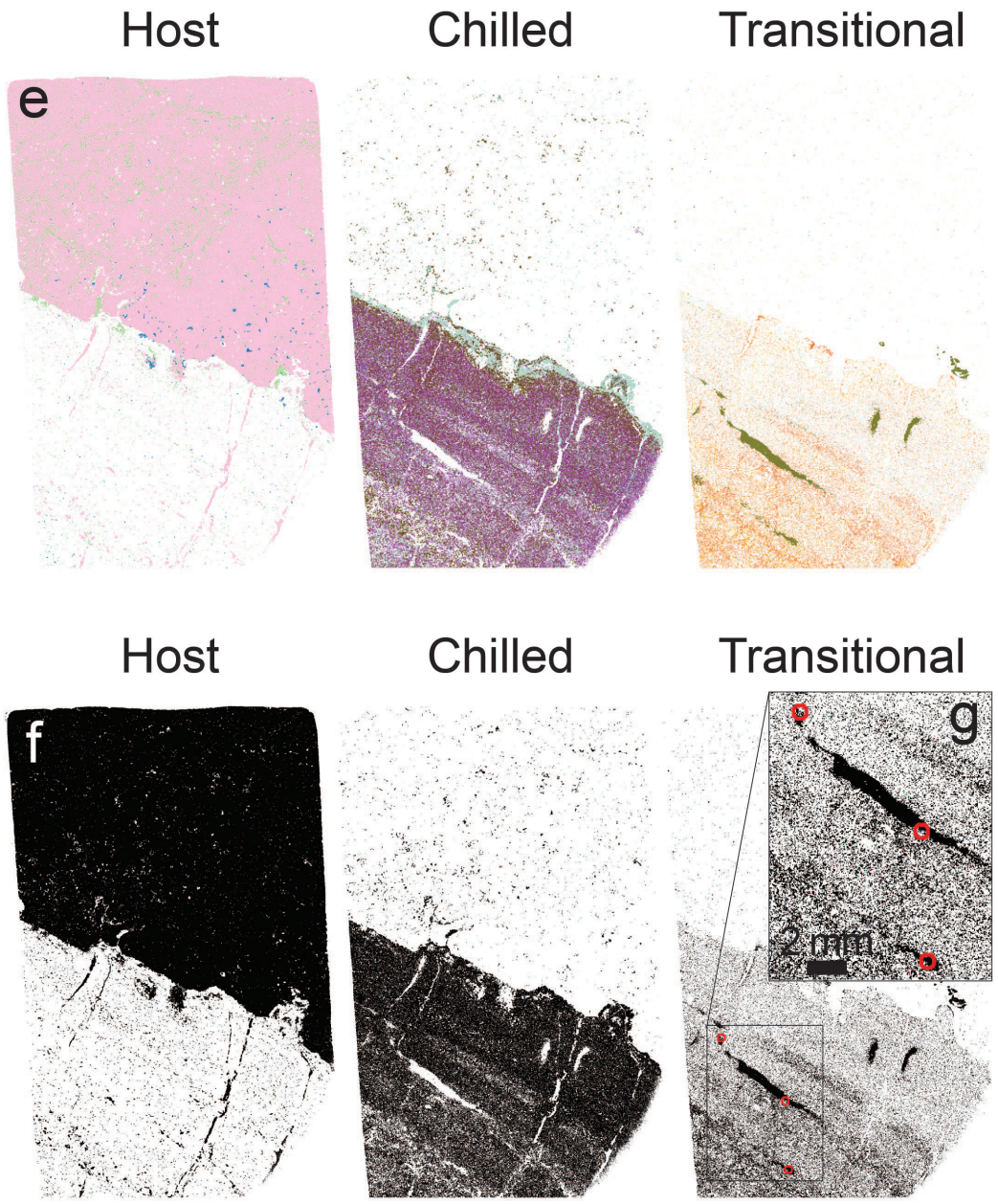

Fig. 4. Continued.

cuprite (Figs. 11a, b) and electrum is primarily observed in secondary Co-As-hydroxide and iron-oxide minerals (Figs. 11c, d). Cobaltite mineralization was not observed in massive sulphide bodies.

5.2. Alteration in igneous and siliciclastic rocks

Skarn and other alteration types in Vancouver Island and Texada Island irons skarns are mostly in igneous and siliciclastic rocks (Webster and Ray, 1990a, b). Carbonate rocks accommodate a much smaller volume of alteration and iron oxide mineralization and are mostly recrystallized into coarse calcite (Bain and Waugh, 2024).

5.2.1. Skarn

Skarn zones consist of masses of prograde garnet-clinopyroxene-anorthite overprinted by retrograde carbonate, quartz, epidote, hornblende, and minor amounts of other Fe-rich amphiboles (Fig. 12). This alteration is texturally destructive, and forms massive garnet skarn composed of course, euhedral grossular garnet with andradite growth zones and intergranular carbonate (Fig. 12b). Masses of prograde skarn typically grade outward from massive garnet to zones of clinopyroxene-anorthite surrounded by fresh host rock (Figs. 12a, b). In porphyritic Karmutsen Formation mafic volcanic host rocks, this alteration forms zones of coarse garnet surrounded by a gradational halo of clinopyroxene that overprints magnetite-

Unique Colour	Custom colour	Mineral	Group
		Apatite	Acs
		Monazite-(Ce)	Acs
		Rutile	Acs
		Titanite	Acs
		Zircon	Acs
		Ferriprehnite	Amp
		Kaersutite	Amp
		Tremolite	Amp
		Chlorite	Alt
		Epidote	Alt
		Gonyerite	Alt
		Scapolite	Ca-Na alt
		Ankerite	Carb
		Calcite	Carb
		Siderite	Carb
		Ag Telluride	CM
		Bi Telluride	CM
		Bismuth	CM
		Co-As Hydroxide	CM
		Cobaltite	CM
		Electrum	CM
		Hg Telluride	CM
		Clinopyroxene	Cpx
		Augite	Cpx
		Andradite	Grt
		Grossular	Grt

Unique Colour	Custom colour	Mineral	Group
		Hedenbergite	Hbl
		Hornblende	Hbl
		Biotite	Mica
		Muscovite	Mica
		Ferrosilite	Opx
		Orthopyroxene	Opx
		Ilmenite	Oxide
		Limonite	Oxide
		Magnetite	Oxide
		Scorodite	Oxide
		Spinel (Cr-Fe)	Oxide
		Quartz	Qtz
		Albite	Spar
		Anorthite	Spar
		Orthoclase	Spar
		Plag 50-50	Spar
		Arsenopyrite	Sulphide
		Bornite	Sulphide
		Chalcocite	Sulphide
		Chalcopyrite	Sulphide
		Cuprite	Sulphide
		Galena	Sulphide
		Pentlandite	Sulphide
		Pyrite	Sulphide
		Pyrrhotite	Sulphide
		Sphalerite	Sulphide

Fig. 5. Colour scheme for SEM-MLA data. Acs = Accessory; Amp = Amphibole; Alt 1 = Early alteration; Ca-Na Alt = Sodic-calcic alteration; Carb = Carbonate; CM = Other critical minerals; Cpx = Clinopyroxene; Grt = Garnet; Hbl = Hornblende; Opx = Orthopyroxene; Qtz = Quartz; Spar = Feldspar.

bearing host rock groundmass and surrounds anorthite-altered primary intermediate plagioclase phenocrysts (Figs. 12c, d).

Skarn zones typically lack discrete Co- and Te-bearing mineral phases unless overprinted by podiform sulphides or magnetite skarn mineralization. In most cases, overprinting sulphides are intergrown with retrograde carbonate-hornblende-quartz that crosscut grossular garnet along fractures and fills intergranular space (Fig. 13).

5.2.2. Sodic-calcic alteration

Sodic-calcic alteration consists of thin selvage of co-genetic albite-scapolite-clinopyroxene-orthoclase-carbonate developed along the edges of <2-5 mm wide veins. In most cases, the selvage is zoned with a sulphide-bearing albite-rich rim and a clinopyroxene-orthoclase-scapolite-carbonate core (Figs. 14a-d). The mineralogy of the veins associated with this alteration type varies and includes albite-hornblende-carbonate-clinopyroxene, scapolite-clinopyroxene-orthoclase, clinopyroxene-ferriprehnite, and epidote-chlorite-ferriprehnite-carbonate varieties (Figs. 14a, b). This alteration type is not texturally destructive and was exclusively observed in fine-grained mafic igneous host rocks proximal to magnetite-calcite and magnetite skarn orebodies (Fig. 14). Zones of sodic-calcic alteration typically lack primary quartz (Figs. 14e, f) and magnetite (Figs. 14g, h) present in unaltered host rock and are weakly overprinted with carbonate. As a result, hand samples of sodic-calcic altered rocks are nonmagnetic and variably effervesce in hydrochloric acid. This alteration type is not

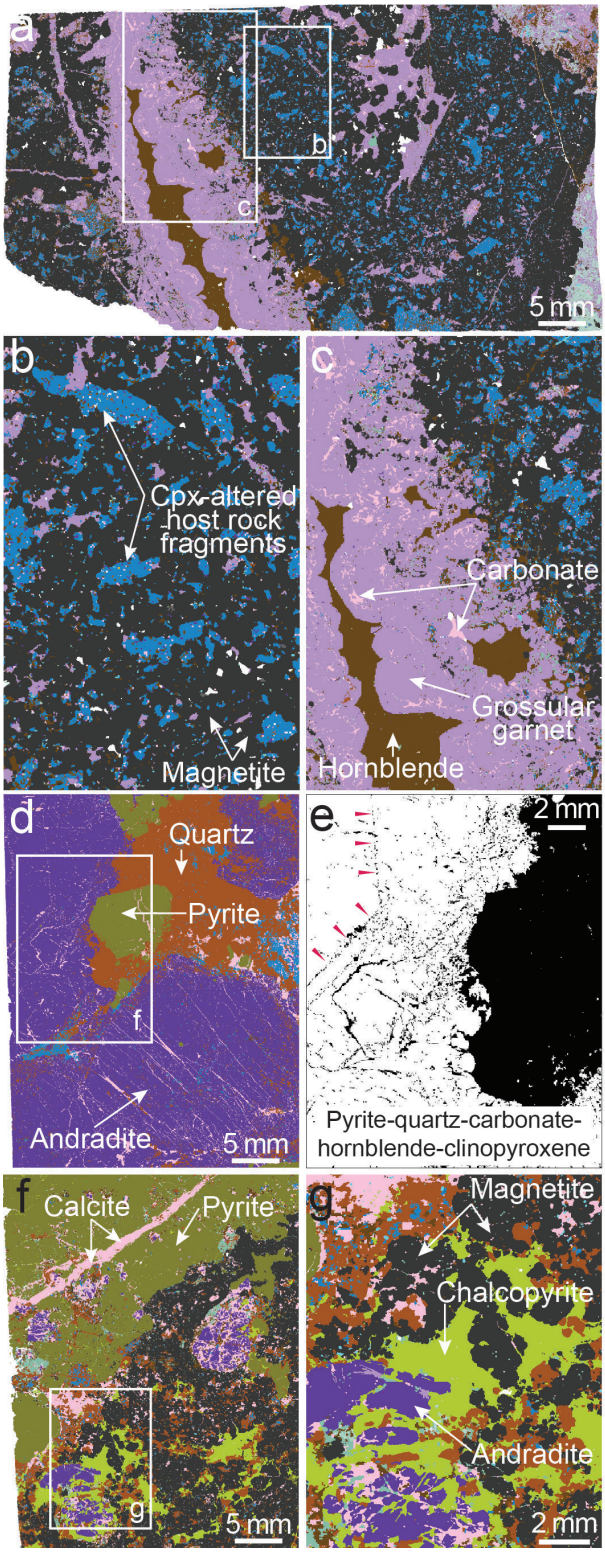

Fig. 6. a) Custom colour MLA image of calc-silicate magnetite skarn mineralization in Karmutsen Formation volcanic rocks from Iron Mike (24WBA-160-24B-3). **b)** Inset image; host rock fragments are pervasively overprinted with clinopyroxene and early-stage chlorite-epidote alteration and are rimmed with coarse- to fine-grained magnetite. **c)** Euhedral grossular (Figs. 7a, c) and intergrown hornblende-carbonate. The garnet in this sample overprints the earlier magnetite-clinopyroxene alteration and fills fractures. **d)** Sulphide-bearing quartz-carbonate-clinopyroxene filling interstitial space between euhedral andradite crystals; calc-silicate magnetite skarn; Prescott occurrence, Texada cluster (S23WBA-78-f). **e)** Distribution of quartz-carbonate-clinopyroxene-pyrite, in black. Carbonate defines growth zones (red arrows) in primary, euhedral, andradite crystals and fills secondary fractures in those same crystals. **f)** and **g)** Sulphide and quartz-carbonate-hornblende-clinopyroxene overprinting magnetite and calc-silicate minerals. Note the fragmentary appearance of early garnet and magnetite.

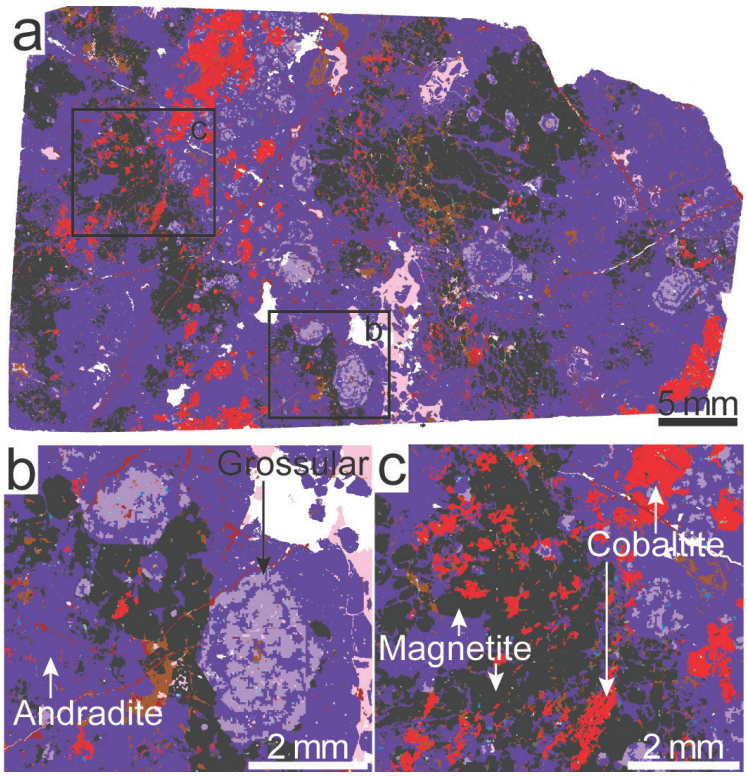

Fig. 7. a) Custom colour MLA image of cobaltite-rich calc-silicate magnetite skarn; Spratt Bay occurrence, Texada cluster (S23WBA-85-c). **b)** Inset image of grossular growth zones in andradite. **c)** Inset image of intergrown magnetite and cobaltite.

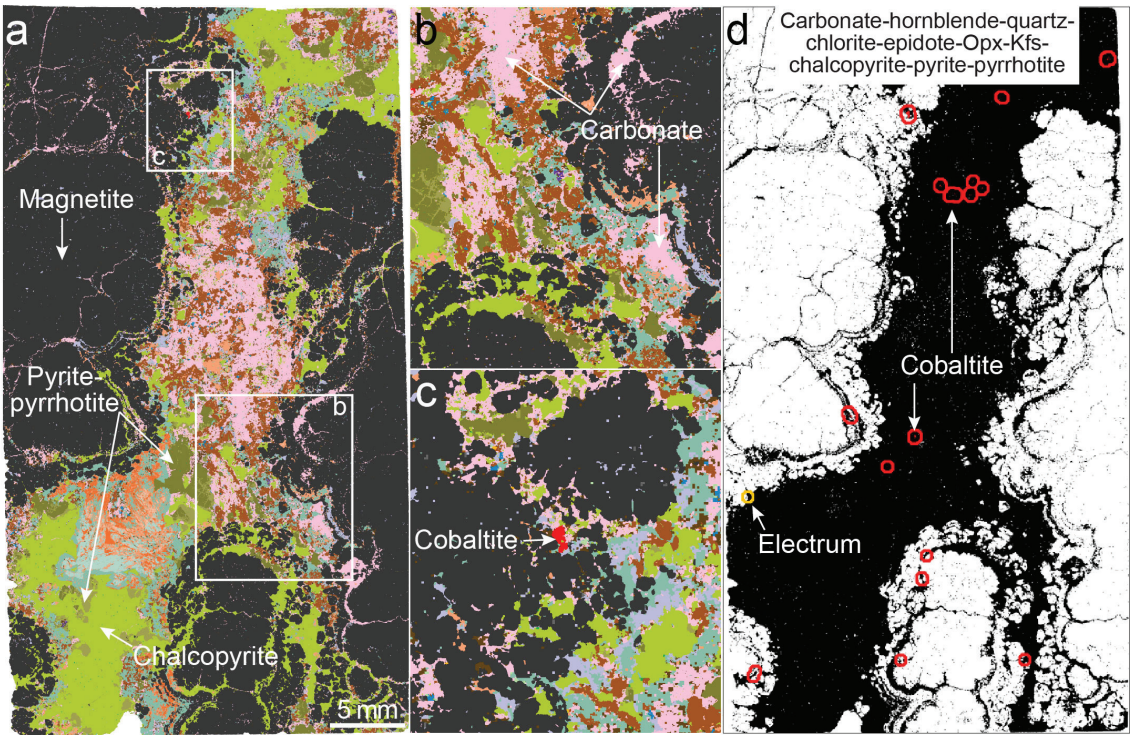

Fig. 8. a) Custom colour MLA image of botryoidal magnetite illustrating open space-filling textures and a central band of sulphide-bearing carbonate-hornblende-quartz-chlorite-epidote-orthopyroxene-orthoclase; Merry Widow deposits, Merry Widow cluster (D23WBA-47-20). **b)** Inset image of gradation from open space-filling botryoidal magnetite to sulphide-bearing carbonate-hornblende-quartz-chlorite-epidote-orthopyroxene-orthoclase. **c)** Inset image of large cobaltite crystal in sulphide-bearing carbonate-hornblende-quartz-epidote-chlorite. **d)** Distribution of cobaltite (circled in red), associated with the carbonate-hornblende-quartz-chlorite-epidote-orthopyroxene (OPX)-orthoclase (Ksp) assemblage (in black).

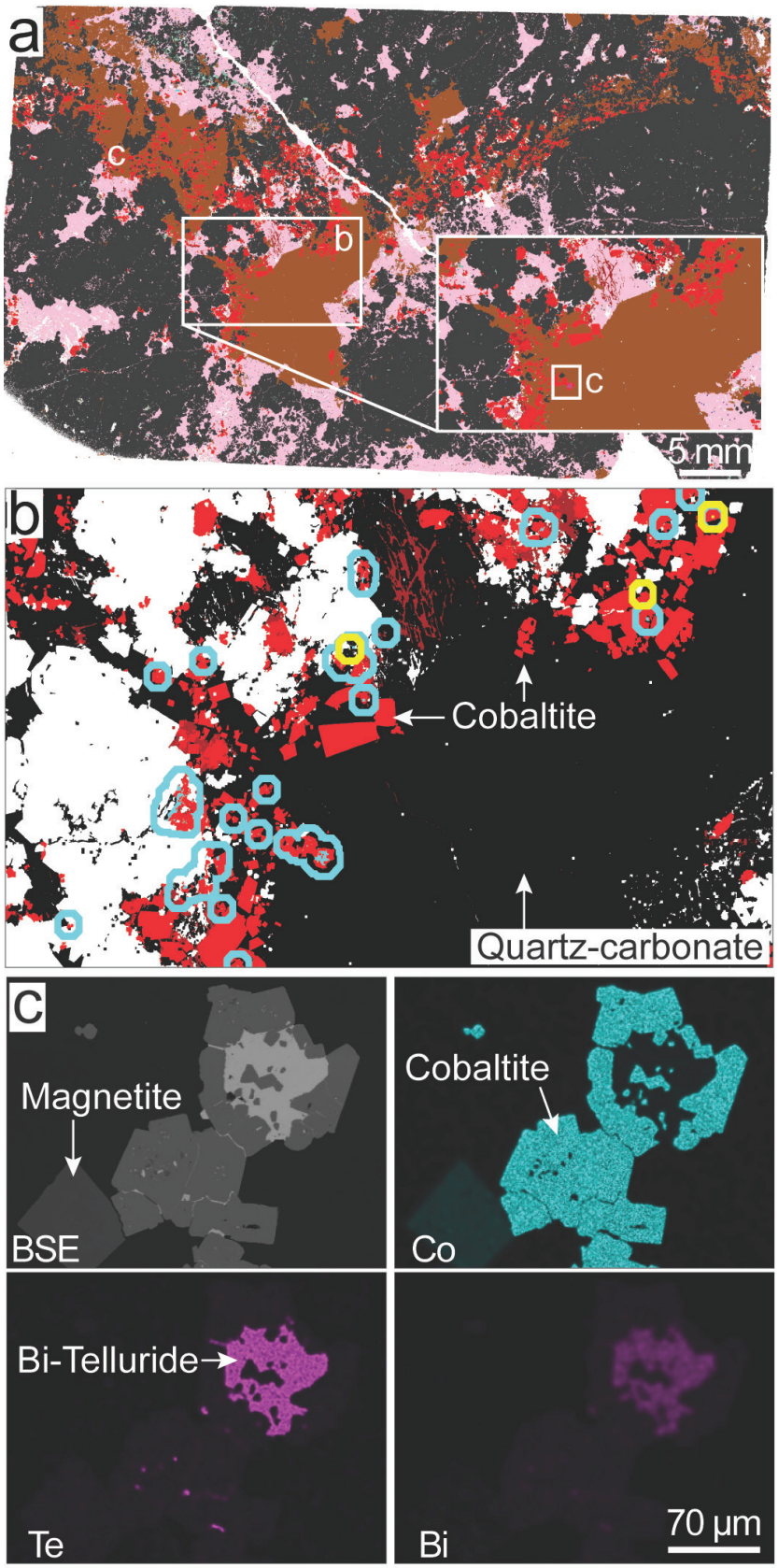

Fig. 9. a) Custom colour MLA image of cobaltite-rich quartz-carbonate gangue cross-cutting magnetite; Bacon Lake deposits, Argonaut cluster (24WBA-157-12A-4). **b)** Inset image of the distribution of quartz-carbonate (black), cobaltite (red), and grains of electrum (circled in yellow) and Ag-Bi telluride (circled in blue). **c)** Inset images of BSE and corresponding element maps for intergrown cobaltite and Bi-telluride.

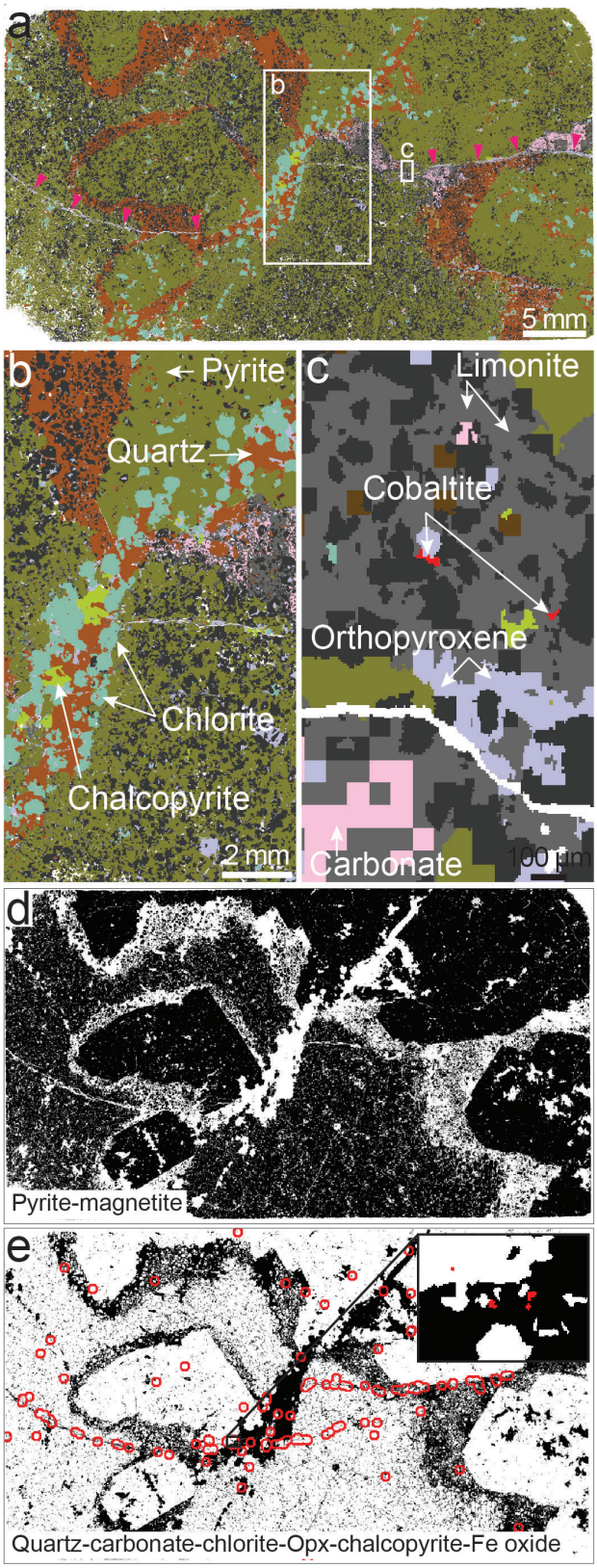

Fig. 10. a-c) Custom colour MLA image of pyrite-rich podiform sulphide mineralization with minor magnetite and cross-cutting quartz-carbonate-chlorite-orthopyroxene-chalcopyrite-limonite assemblage; Iron Mike deposit, Iron Mike cluster (S23WBA-69-a-2). Cobaltite is intergrown with the cross-cutting assemblage. **d)** Distribution of pyrite-magnetite (in black). **e)** Distribution of cross-cutting quartz-carbonate-chlorite-orthopyroxene-chalcopyrite-limonite (in black) and associated cobaltite. Cobaltite grains in this sample are typically small (e.g., Fig. 10c) and are circled in red.

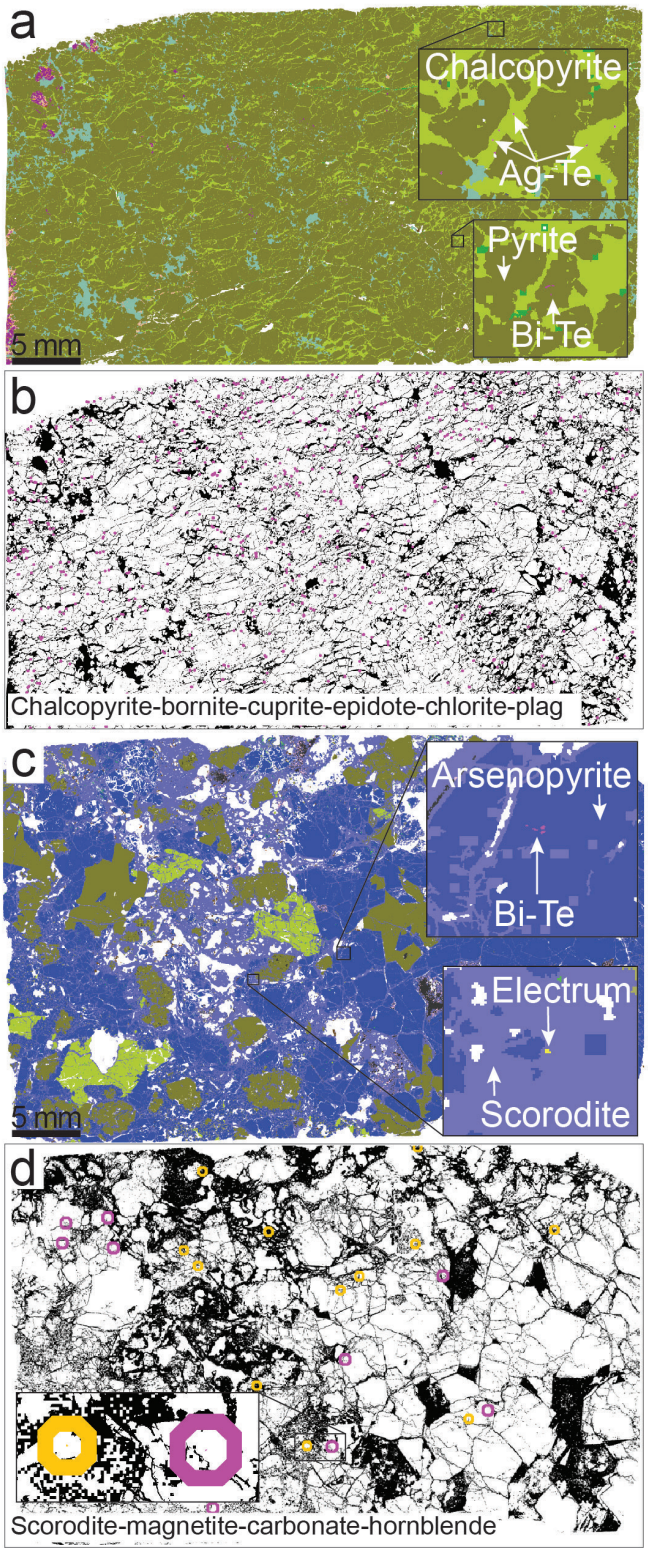

Fig. 11. a) Custom colour MLA image of pyrite-rich massive sulphide crosscut by secondary chalcopyrite-bornite-cuprite-epidote-chlorite-plagioclase; Prescott deposits, Texada cluster (S23WBA-79-c). Plagioclase (plag) in this sample is mostly albite. Inset images show Ag-telluride (Ag-Te) in secondary chalcopyrite and primary pyrite. **b)** Distribution of secondary chalcopyrite-bornite-cuperite-epidote-chlorite-plagioclase, in black. Clusters of Ag-Bi-Hg telluride, like those shown in the inset images of a), are denoted with pink dots. **c)** Custom colour MLA image of arsenopyrite-rich massive sulphide crosscut by secondary scorodite-magnetite-carbonate-hornblende; B3 deposits, Merry Widow cluster (S23WBA-31-a-1). Inset images show Ag-Te in primary arsenopyrite and electrum in secondary scorodite. **d)** Distribution of secondary scorodite-magnetite-carbonate-hornblende (in black), with small electrum grains (circled in yellow) and Ag-Bi-Hg telluride grains (circled in magenta).

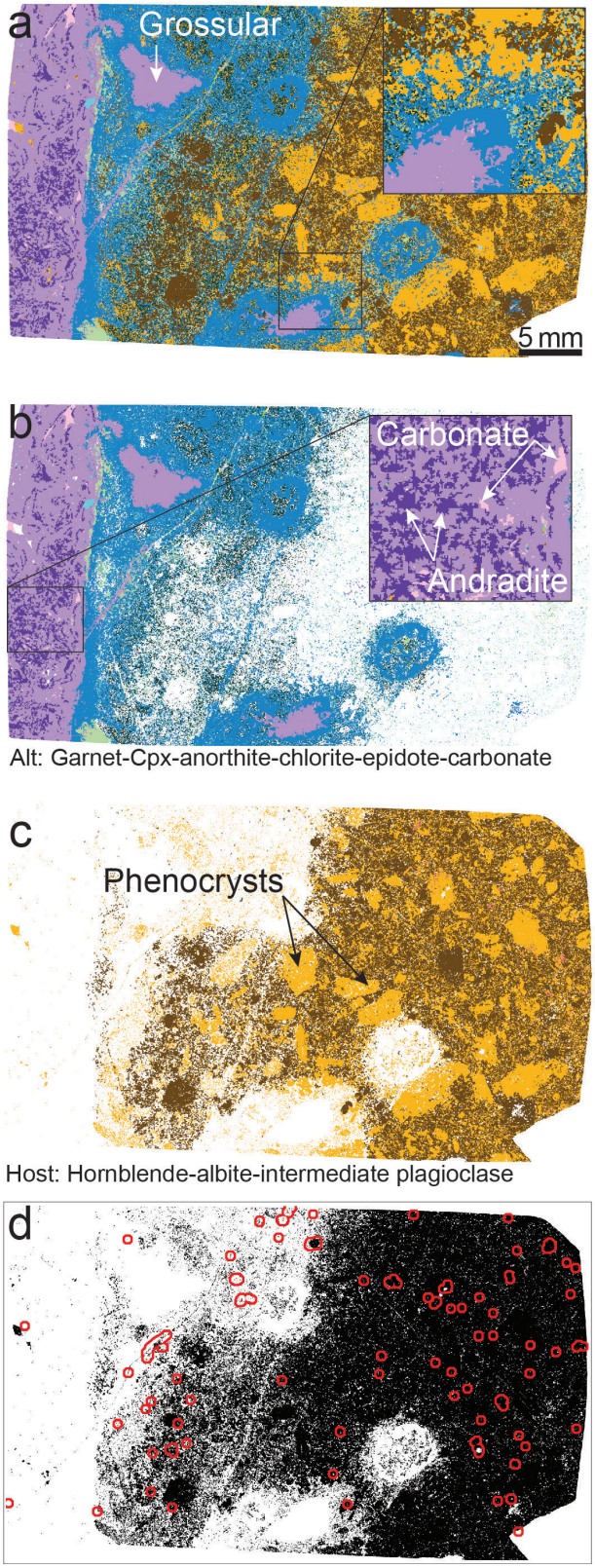

Fig. 12. a) Custom colour MLA image of calc-silicate alteration overprinting porphyritic Karmutsen Formation volcanic host rock, Van Ada deposits, Texada cluster (S23WBA-85-c). Inset image shows the texturally destructive overprint of clinopyroxene-anorthite, followed by garnet on the intermediate plagioclase phenocrysts, and hornblende-rich groundmass. **b)** Garnet-clinopyroxene-anorthite-chlorite-epidote-carbonate alteration assemblage. Inset shows andradite growth zones and interstitial carbonate in massive grossular garnet. **c)** Remnant hornblende-albite-intermediate plagioclase from the host rock. **d)** Distribution of host rock (in black) and primary magnetite crystals (circled in red). Note the abundance of magnetite in the unaltered and partly altered host rocks and its absence in pervasively altered areas.

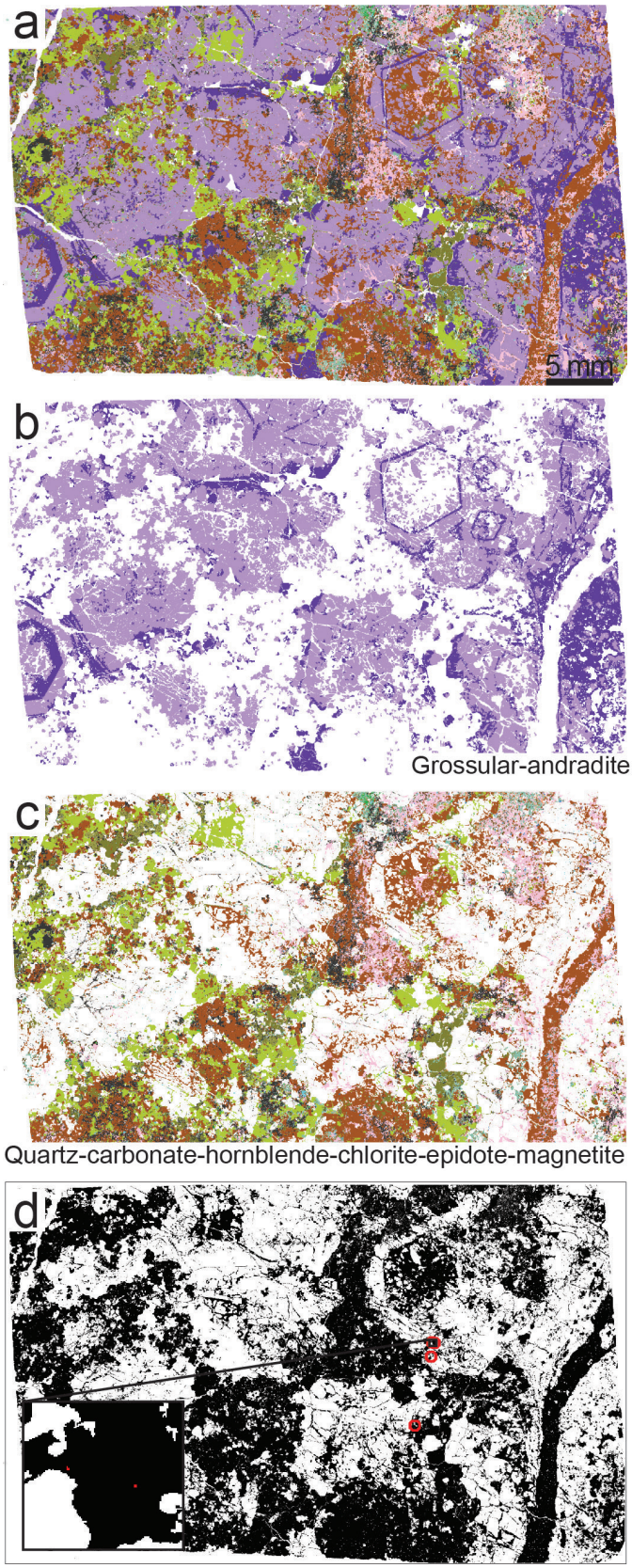

Fig. 13. a) Custom colour MLA image showing sulphides and quartz-carbonate-hornblende-chlorite-epidote-magnetite overprinting calc-silicate alteration, Iron River deposit, Argonaut cluster (S23WBA-21-a-4). **b)** Distribution of coarse grossular-andradite; euhedral pre-existing garnet and andradite-rich growth zones. **c)** Distribution of sulphides (green) and quartz-carbonate-hornblende-chlorite-epidote-magnetite. **d)** Distribution of sulphides and quartz-carbonate-hornblende-chlorite-epidote-magnetite (in black); sparse cobaltite crystals (circled in red).

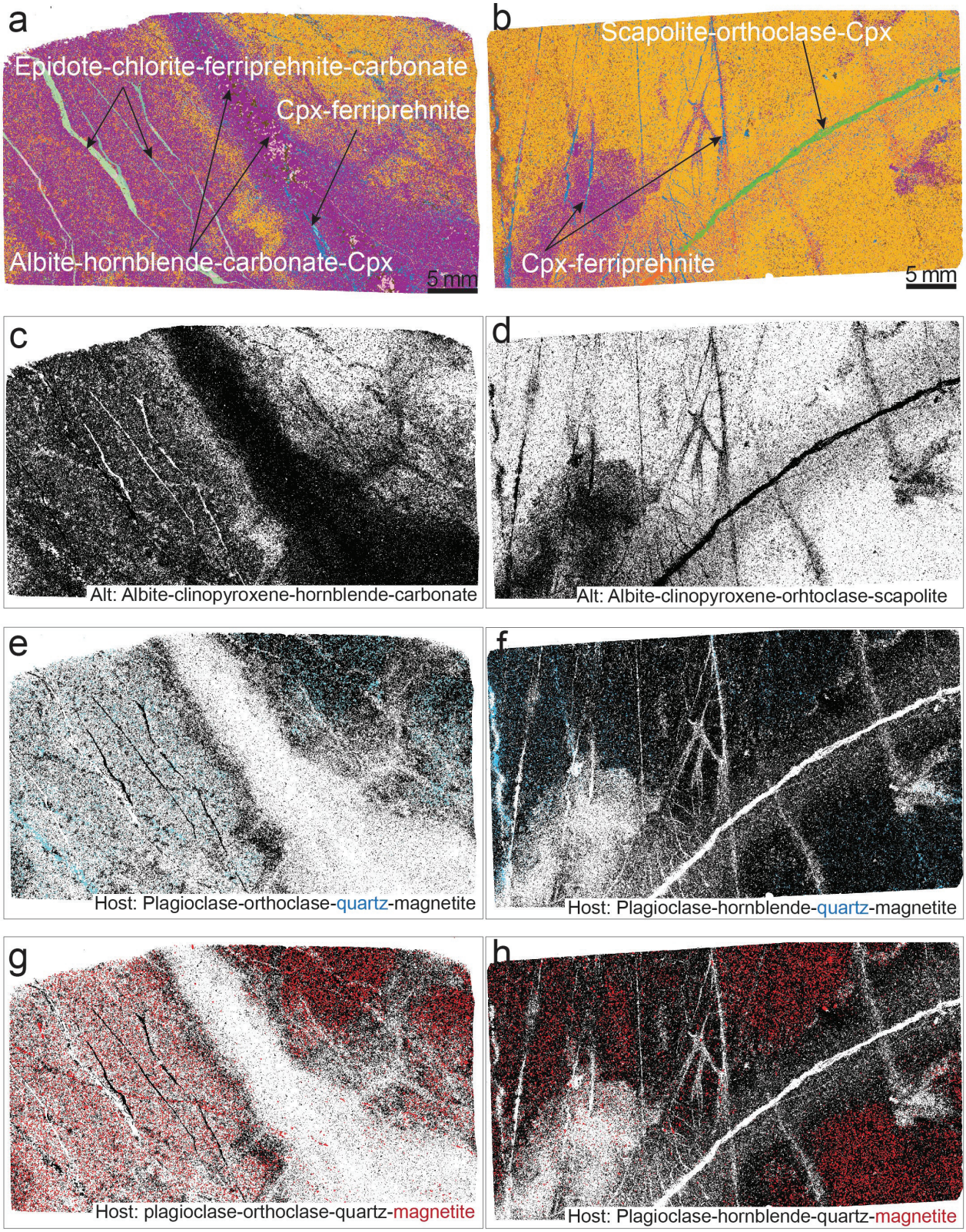

Fig. 14. a, b) Custom colour MLA image showing sodic-calcic alteration around albite-hornblende-carbonate-clinopyroxene, scapolite-clinopyroxene-orthoclase, clinopyroxene-ferriprehnite, and epidote-chlorite-ferriprehnite-carbonate veins in Bonanza Group host rocks, Merry Widow deposit, Merry Widow cluster (a: D23WBA-47-49; b: D23WBA-48-4). **c, d)** Distribution of the sodic-calcic alteration assemblage (albite-clinopyroxene-orthoclase-hornblende-carbonate-scapolite; in black). **e-h)** Distribution of primary host rock mineralogy (intermediate plagioclase-orthoclase-quartz-magnetite; in black); quartz **e)**, **f)** in blue and magnetite **g), h)** in red; pixels have been enlarged. Quartz and magnetite are absent in areas overprinted with sodic-calcic alteration.

associated with Co- or Te-bearing mineral phases but has a clear spatial association with magnetite- and sulphide-bearing ore bodies.

6. Discussion

6.1. Co and Te minerals in Vancouver Island and Texada Island iron skarns

The iron skarns evaluated in this study contain variable amounts of Co in primary Co-arsenides, sulphoarsenides (e.g., cobaltite), and secondary Co-As hydroxide minerals. Like the primary base-metals sulphides, Co-bearing minerals are commonly associated with retrograde calcite-hornblende-quartz and are generally absent from prograde magnetite mineralization. The only exception is the prograde magnetite skarn mineralization in limestones in the upper part of the Karmutsen Formation on Texada Island (e.g., Spratt Bay), where coarse cobaltite is intergrown with prograde magnetite and garnet (Fig. 7). This is one of the few cases where calc-silicate alteration and iron skarn mineralization are more abundant in carbonate host rocks than the surrounding mafic igneous rocks. In general, Karmutsen Formation rocks, volcanic and sedimentary, are more consistent host rocks for Co-bearing mineralization relative to the Bonanza Group, Quatsino Formation, or Island Plutonic suite intrusions. This suggests that the occurrence of Co mineralization is a function of host rock compositions.

Tellurium mineralization is also typical in sulphide mineralization in the iron skarns we studied, regardless of its deposit-scale setting. This mineralization occurs primarily as Ag-Bi-Hg telluride inclusions in pyrite, pyrrhotite, chalcopyrite, and arsenopyrite and occurs with native bismuth and electrum. These inclusions are most abundant in chalcopyrite-rich massive sulphides (e.g., B3; Fig. 11) and where tellurides and electrum occur with cobaltite in late-stage calcite-hornblende-quartz (e.g., Bacon Lake; Fig. 9). In addition, it is common for Au-Ag to concentrate in supergene environments (Burisch et al., 2017; Burisch et al., 2019), and this is likely to be the case for the electrum mineralization concentered in gossans and other weathering products of massive sulphides observed in the studied deposits (Fig. 11c). These observations highlight a distinctive setting of Te and Au-Ag mineralization across all iron skarns on Vancouver Island and Texada Island.

6.2. Alteration at iron skarns on Vancouver Island and Texada Island

The occurrence of pervasive skarn alteration in igneous and siliciclastic rock types is a key distinction that sets Wrangel terrane iron skarns apart from metasomatic skarn varieties (Meinert et al., 2005). Although not consistently enriched in Co-Te-Bi mineralization, andradite-rich garnet skarn is commonly spatially associated or intergrown with primary magnetite and sulphide mineralization. In contrast, grossular-rich calc-silicate alteration contains little to no primary mineralization and is typically distal from mineralized zones relative to andradite-rich alteration. These patterns are consistent across all the surveyed deposits.

Sodic-calcic alteration commonly crosscuts host rocks along the peripheries of iron skarns described in this study. For instance, the Merry Widow orebody is surrounded by pale-green sodic-calcic alteration developed along scapolite-orthoclase-clinopyroxene-carbonate veins cross-cutting Parson Bay Formation volcanic rocks. The formation of this alteration involves the conversion of feldspar group minerals to anorthite (early) and albite (late), a minor overprint of clinopyroxene-orthoclase-carbonate, and the absence of primary quartz and magnetite in the altered host rock. Based on these characteristics, the formation of sodic-calcic alteration likely involves the metasomatic addition of Na, Ca, and CO_3^{2-} and the destruction of quartz and Fe-oxide in the affected host rocks.

7. Conclusion

The data presented here describes the occurrence of Co and Te minerals in iron skarns on Vancouver Island and Texada Island and highlights common features. These features include: 1) Fe-rich skarn formed in volcanic and siliciclastic rocks in the upper part of the Karmutsen Formation and the lower part of the Bonanza Group; 2) zones of quartz- and magnetite-destructive sodic-calcic alteration that form peripheral to skarn bodies and zones of calc-silicate alteration; 3) a ubiquitous association between sulphide mineralization and retrograde calcite-hornblende-quartz cross-cutting prograde magnetite; and 4) massive sulphide bodies hosted in recrystallized limestone. This dataset also highlights a suite of elements (Co, Te, Bi) that could conceivably be produced as by-products in deposits with economic Cu, Au-Ag, and Fe mineralization. These metals commonly concentrate in the weathering products of the sulphide orebodies and could be evaluated as geochemical indicators for iron skarn mineralization in soil surveys.

Acknowledgments

We thank Evan Orovan (BCGS), Luke Ootes (BCGS), Jeffrey Chiarenzelli (St. Lawrence University), and Mathias Burisch Hassel (Colorado School of Mines) for reviews that substantially improved this paper. Sam Waugh helped with data preparation and fieldwork. Paulina Marczak (BCGS) and Kaitlyn McLaren (BCGS) provided geographic information system support. Del Ferguson (Aztec Geoscience), Adam Travis, and Jesse Collison (Coast Copper Corp.) helped us access the Argonaut and Merry Widow clusters.

References cited

Bain, W.M., and Waugh, S.A.F., 2024. Ore and alteration textures of limestone-hosted magnetite-sulphide mineralization at the Merry Widow deposit, Vancouver Island, British Columbia. In: Geological Fieldwork 2023, British Columbia Ministry of Energy, Mines and Low Carbon Innovation, British Columbia Geological Survey GeoFile 2024-15, 14 p.

Beranek, L.P., Hutter, A.D., Pearcey, S., James, C., Langor, V., Pike, C., Goudie, D., and Oldham, L., 2023. New evidence for the Baltican cratonic affinity and Tonian to Ediacaran

tectonic evolution of West Avalonia in the Avalon Peninsula, Newfoundland, Canada. Precambrian Research, 390. <https://doi.org/10.1016/j.precamres.2023.107046>

Bird, S., 2023. NI 43-101 Resource estimate update for the Merry Widow deposits, Empire Mine property. NI 43-101 Technical Report, 101 p. Available from: <http://sedar.com/>

Burisch, M., Gerdes, A., Walter, B.F., Neumann, U., Fettel, M., and Markl, G., 2017. Methane and the origin of five-element veins: Mineralogy, age, fluid inclusion chemistry and ore forming processes in the Odenwald, SW Germany. Ore Geology Reviews, 81, 42-61.

Burisch, M., Gerdesb, A., Meinert, L.D., Albert, R., Seiferta, T., and Gutzmer, J., 2019. The essence of time-fertile skarn formation in the Variscan Orogenic Belt. Earth and Planetary Science Letters, 519, 165-170.

Colpron, M., 2020. Yukon Terranes-A digital atlas of terranes for the northern Cordillera. Yukon Geological Survey. <data.geology.gov.yk.ca/Compilation/2#InfoTab>

Canil, D., and Morris, R.A., 2024. Continentalization of an intraoceanic arc as exemplified by the Jurassic Bonanza arc of Vancouver Island, Canada. Geological Society of America Bulletin 136, 880-892. <https://doi.org/10.1130/B36716.1>

Canil, D., Styan, J., Larocque, J., Bonnet, E., and Kyba, J., 2010. Thickness and composition of the Bonanza arc crustal section, Vancouver Island, Canada. Geologic Society of America Bulletin, 122, 1094-1105.

Cox, D.P., 1986. Descriptive model of Fe skarn deposits. In: Cox, D.P., and Singer, D.A., (Eds), Mineral deposit models: U.S. Geological Survey Bulletin 1693, p. 94.

Cui, Y., Miller, D., Schiarizza, P., and Diakow, L.J., 2017. British Columbia digital geology. British Columbia Ministry of Energy, Mines and Petroleum Resources, British Columbia Geological Survey Open File 2017-8, 9 p. Data version 2019-12-19.

Dawson, K.M., and Kirkham, R.V., 1996. Skarn copper. In: Eckstrand, O.R., Sinclair, W.D., and Thorpe, R.I., (Eds.), Geology of Canadian Mineral Deposit Types. Geological Survey of Canada, Geology of Canada, 8, pp. 460-476.

DeBari, S.M., Anderson, R.G., and Mortensen, J.K., 1999. Correlation among lower to upper crustal components in an island arc: The Jurassic Bonanza arc, Vancouver Island, Canada. Canadian Journal of Earth Sciences, 36, 1371-1413.

Dehaine, Q., Tijsseling, L.T., Glass, H.J., Törmänen, T., and Butcher, A.R., 2021. Geometallurgy of cobalt ores: A review. Minerals Engineering. <https://doi.org/10.1016/j.mineng.2020.106656>

Einaudi, M.T., Meinert, L.D., and Newberry, R.J., 1981. Skarn deposits. In: Skinner, B.J., (Eds.), Economic Geology, 75th-Anniversary volume, pp. 317-391.

Ettlinger, A.D., and Ray, G.E., 1989. Precious metal enriched skarns in British Columbia: An overview and geological study. British Columbia Ministry of Energy, Mines and Petroleum Resources, British Columbia Geological Survey Paper 1989-03, pp. 1-128.

Ferguson, D.W., 2021. Report on 2020-2021 exploration mineral tenures 1082812, 1082824, 1082825, 1082826 Bacon Lake Property, Nanaimo Mining Division, BC. Western Gateway Minerals Inc., British Columbia Ministry of Energy and Mines, British Columbia Geological Survey Assessment Report 39537, 52 p.

Goldfarb, R., 2015. Tellurium-The bright future of solar energy. U.S. Geological Survey Fact Sheet 2014-3077. <https://dx.doi.org/10.3133/fs20143077>

Grant, D.C., Goudie, D.J., Voisey, C., Shaffer, M., and Sylvester, P., 2018. Discriminating hematite and magnetite via Scanning Electron Microscope-Mineral Liberation Analyzer in the -200 mesh size fraction of iron ores. Applied Earth Science, 127, 30-37. <https://doi.org/10.1080/03717453.2017.1422334>

Greene, A.R., Scoates, J.S., Nixon, G.T., and Weis, D., 2006. Picritic lavas and basal sills in the Karmutsen flood basalt province, northern Vancouver Island. In: Geological Fieldwork 2005, British Columiba Ministry of Energy, Mines and Petroleum Resources, Paper 2006-1, pp. 39-51.

Hancock, K.D., 1998. Magnetite occurrences in British Columbia. British Columbia Ministry of Energy, Mines and Petroleum Resources, British Columbia Geological Survey Open File 1998-28, 153 p.

Hickin, A.S., Ootes, L., Orovan, E.A., Brzozowski, M.J., Northcote, B.K., Rukhlov, A.S., and Bain, W.M., 2024. Critical minerals and mineral systems in British Columbia. In: Geological Fieldwork 2023, British Columbia Ministry of Energy, Mines and Low Carbon Innovation, British Columbia Geological Survey Paper 2024-01, pp.13-51.

Kesler, S.E., 1968. Contact-localized ore formation in the Memé mine, Hait. Economic Geology, 63, 541-552.

Lapham, D.M., 1968. Triassic magnetite and diabase at Cornwall, Pennsylvania. In: Ore deposits of the United States 1937-1967, The Graton-Sales volume, York, Pennsylvania, The Maple Press Co., v. I, p. 73-94.

Liang, X., Wang, F., Zhang, L., Zhang, J., Wei, C., Fan, Y., Guo, X., Zhou, T., Zhang, J., and Lü, Q., 2023. Cobalt distribution and enrichment in skarn iron deposits: A case study of the Zhuchong skarn iron deposit, Eastern China. Ore Geology Reviews. <https://doi.org/10.1016/j.oregeorev.2023.105778>

Massey, N.W.D., 1995a. Geology and mineral resources of the Alberni-Nanaimo lakes sheet, Vancouver Island, 92F/01W, 92F/02E and part of 92F/07E; British Columbia Ministry of Energy, Mines and Petroleum Resources, British Columbia Geological Survey Paper 1992-02, 132 p.

Massey, N.W.D., 1995b. Geology and mineral resources of the Cowichan Lake sheet, Vancouver Island, 92C/16. British Columbia Ministry of Energy, Mines and Petroleum Resources, British Columbia Geological Survey Paper 1992-03, 112 p.

Massey, N.W.D., 1995c. Geology and mineral resources of the Duncan sheet, Vancouver Island, 92B/13. British Columbia Ministry of Energy, Mines and Petroleum Resources, British Columbia Geological Survey Paper 1992-04, 112 p.

Meinert, L.D., Dipple, G.M., and Nicolescu, S., 2005. World skarn deposits. In: Hedenquist, J.W., Thompson, J.F.H., Goldfarb, R.J., and Richards, J.P., (Eds.), Economic Geology, 100th Anniversary volume, pp. 299-336.

Morris, R.A., and Canil, D., 2020. Skarn mineralization along magma-carbonate contacts in the Merry Widow Mountain area, Vancouver Island, British Columbia (NTS 092L). In: Geoscience BC Summary of Activities 2019: Minerals, Geoscience BC, Report 2020-01, pp. 5-12.

Morris, R.A., and Canil, D., 2024. Crust-derived CO_2 production from a shallow pluton in limestone is driven by metamorphic decarbonation, not assimilation. Geochemistry, Geophysics, Geosystems, 25, article e2024GC011485. <https://doi.org/10.1029/2024GC011485>

Mudd, G.M., Weng, Z., Jowitt, S.M., Turnbull, I.D., and Graedel, T.E., 2013. Quantifying the recoverable resources of by-product metals: The case of cobalt. Ore Geology Reviews, 55, 87-98.

Nassar, N.T., Lederer, G.W., Brainard, J.L., Padilla, A.J., and Lessard, J.D., 2022. Rock-to-metal ratio: A foundational metric for understanding mine wastes. Earth, Science, and Technology, 56, 6710-6721.

Newberry, R.J., 1991. Scheelite-bearing skarns in the Sierra Nevada region, California. Contrasts in zoning and mineral compositions and tests of infiltration metasomatism theory. In: Barto-Kyriakidis, A., (Eds)., Skarns-Their Genesis and Metallogeny, Theophrastus Publications, Athens, Greece, pp. 343-384.

Nixon, G.T., and Orr, A.J., 2007. Recent revisions to the early Mesozoic stratigraphy of Vancouver Island and metallogenic implications. British Columbia. In: Geological Fieldwork 2006, British Columbia Ministry of Energy, Mines and Petroleum Resources, British Columbia Geological Survey Paper 2007-1, pp. 163-177.

Nixon, G.T., Hammack, J.L., Hamilton, J.V., Jennings, H., Larocque, J.P., Orr, A.J., Friedman, R.M., Archibald, D.A., Creaser, R.A., Orchard, M.J., Haggart, J.W., Tipper, H.W., Tozer, E.T., Cordey, F., and McRoberts, C.A., 2011a. Geology, geochronology, lithogeochemistry and metamorphism of the Mahatta Creek area, northern Vancouver Island. British Columbia Ministry of Energy and Mines, British Columbia Geological Survey Geoscience Map 2011-03, 1:50,000 scale.

Nixon, G.T., Hammack, J.L., Koyanagi, V.M., Payie, G.J., Orr, A.J., Haggart, J.W., Orchard, M.J., Tozer, E.T., Friedman, R.M., Archibald, D.A., Palfy, J., and Cordey, F., 2011b. Geology, geochronology, lithogeochemistry and metamorphism of the Quatsino-Port McNeill area, northern Vancouver Island. British Columbia Ministry of Energy and Mines, British Columbia Geological Survey Geoscience Map 2011-02, 1:50,000 scale.

Nixon, G.T., Hammack, J.L., Koyanagi, V.M., Snyder, L.D., Payie, G.J., Panteleyev, A.,Massey, N.W.D., Hamilton, J.V., Orr, A.J., Friedman, R.M., Archibald, D.A., Haggart, J.W., Orchard, M.J., Tozer, E.T., Tipper, H.W., Poulton, T.P., Palfy, J., and Cordey, F., 2011c. Geology, geochronology, lithogeochemistry, and metamorphism of the Holberg-Winter Harbour area, northern Vancouver Island. British Columbia Ministry of Energy and Mines, British Columbia Geological Survey Geoscience Map 2011-01, 1:50,000 scale.

Nixon, G.T., Snyder, L.D., Payie, G.J., Long, S., Finnie, A., Orr, A.J., Friedman, R.M., Archibald, D.A., Orchard, M.J., Tozer, E.T., Poulton, T.P., and Haggart, J.W., 2011d. Geology, geochronology, lithogeochemistry and metamorphism of the Alice Lake area, northern Vancouver Island. British Columbia Ministry of Energy and Mines, British Columbia Geological Survey Geoscience Map 2011-04, 1:50,000 scale.

NRCan (Natural Resources Canada), 2024. Critical Minerals List. Government of Canada. <https://www.canada.ca/en/campaign/critical-minerals-in-canada/critical-minerals-an-opportunity-for-canada.html> (last accessed December 27, 2024).

Ray, G.E., and Webster, I.C.L., 1991. Geology and mineral occurrences of the Merry Widow skarn camp, northern Vancouver Island, 92L/06. British Columbia Ministry of Energy, Mines and Petroleum Resources, British Columbia Geological Survey Open File 1991-8, 1:5000 scale.

Ray, G.E., and Webster, I.C.L, 2007. Geology and chemistry of the low-Ti magnetite-bearing Heff Cu-Au skarn and its associated plutonic rocks, Heffley Lake, south-central British Columbia. Exploration and Mining Geology, 16, 159-167.

Ray, G.E., 2013. A review of skarns in the Canadian Cordillera. British Columbia Ministry of Energy and Mines, British Columbia Geological Survey, Open-File 2013-08, 50 p.

Sangster, D.F., 1969. The contact metasomatic magnetite deposits of British Columbia. Geological Survey of Canada, Bulletin 172, 85 p.

Shan. P., Cao, M., Evans, N.J., Gao, H., Mao, Y., Gao, Y., Salazar, L., Zhao, Y., and Qin, K., 2023. Automated quantitative mineralogy analysis reveals characteristics of Co occurrences in the Jinchang porphyry deposit, NE China. Ore Geology Reviews. <https://doi.org/10.1016/j.oregeorev.2023.105524>

Shearer, J.T., 2007. Geological and metallurgical report on the Iron Ross project. Eagle Industrial Minerals, British Columbia Ministry of Energy and Mines, British Columbia Geological Survey Assessment Report 29186, 67 p.

Slack, J.F., Kimball, B.E., and Shedd, K.B., 2017. Cobalt. In: Schulz, K.J., DeYoung, J.H., Seal, R.R., and Bradley, D.C., (Eds.), Critical Mineral Resources of the United States-Economic and Environmental Geology and Prospects for Future Supply Reston, pp. F1-F40. <https://doi.org/https://doi.org/10.3133/pp1802F>

Sutherland Brown, A., 1968. Geology of the Queen Charlotte Islands. British Columbia Ministry of Energy, Mines and Petroleum Resources Bulletin 54, 226 p.

Sylvester, P.J., 2012. Use of the mineral liberation analyzer (MLA) for mineralogical studies of sediments and sedimentary rocks. In: Sylvester, P., (Eds.), Quantitative Mineralogy and Microanalysis of Sediments and Sedimentary Rocks: Mineralogical Association of Canada Short Course 42. Quebec, Canada, pp. 1-16.

Travis, A., Collison, J., Paynton, B., Sadurski, A., and Vis, D., 2022. Geologic, Geochemical, Geophysical, Prospecting, and Drilling Assessment Report. Tripoint Geological Services, Technical Report, 72 p. Available from: <http://sedar.com/>

USGS, 2024. Mineral Commodity Summaries-Cobalt. Reston, Virginia. <https://doi.org/10.3133/mcs2024>

Vidal, C.E., Injoque-Espinoza, J., Sidder, G.B., and Mukasa, S.B., 1990. Amphibolitic Cu-Fe skarn deposits in the central coast of Peru. Economic Geology, 85, 1447-1461.

Wang, S., Cao, M., Li, G., Silang, W., Shan, P., and Qin, K., 2022a. The occurrence of cobalt and implications for the genesis of the Pusangguo cobalt-rich skarn deposit in Gangdese, Tibet. Ore Geology Reviews, 150, article 105193. <https://doi.org/10.1016/j.oregeorev.2022.105193>

Wang, Z., Wang, Y., Peng, E., Zou, S., Deng, T., Lai, F., Ning, J., Dong, G., and Xu, D., 2022b. Micro-textural and chemical fingerprints of hydrothermal cobalt enrichment in the Jingchong Co-Cu polymetallic deposit, South China. Ore Geology Reviews, 142, article 104721. <https://doi.org/10.1016/j.oregeorev.2022.104721>

Webster, I.C.L., and Ray, G.E., 1990a. Geology and mineral deposits of northern Texada Island. British Columbia Ministry of Energy, Mines and Petroleum Resources Paper 1990-1, pp. 257-265.

Webster, I.C.L., and Ray, G.E., 1990b. Geology and mineral deposits of northern Texada Island. British Columbia Ministry of Energy, Mines and Petroleum Resources Open File 1990-3.

Zarayskiy, G.P., Zharikov, V.A., Stoyanovskaya, F.M., and Balashov, V.N., 1987. The experimental study of bimetasomatic skarn formation: International Geology Review, 29, 761-858.

Zharikov, V.A., 1970a. Skarns, part I. International Geology Review, 12, 541-559.

Zharikov, V.A., 1970b. Skarns, part II. International Geology Review, 12, 619-647.